Neutrino many-body flavor evolution: The full Hamiltonian

Vincenzo Cirigliano,[1] Srimoyee Sen,[2] and Yukari Yamauchi[1]
[1]*Institute for Nuclear Theory, University of Washington, Seattle, Washington 98195, USA*
[2]*Department of Physics and Astronomy, Iowa State University, Ames, Iowa, 50011, USA*

(Received 21 May 2024; accepted 17 October 2024; published 20 December 2024)

We study neutrino flavor evolution in the quantum many-body approach using the full neutrino-neutrino Hamiltonian, including the usually neglected terms that mediate nonforward scattering processes. Working in the occupation number representation with plane waves as single-particle states, we explore the time evolution of simple initial states with up to $N = 10$ neutrinos. We discuss the time evolution of the Loschmidt echo, one body flavor and kinetic observables, and the one-body entanglement entropy. For the small systems considered, we observe "thermalization" of both flavor and momentum degrees of freedom on comparable time scales, with results converging towards expectation values computed within a microcanonical ensemble. We also observe that the inclusion of nonforward processes generates a faster flavor evolution compared to the one induced by the truncated (forward) Hamiltonian.

DOI: 10.1103/PhysRevD.110.123028

I. INTRODUCTION

The evolution of neutrino flavor in hot and dense media provides key input to our understanding of the synthesis of light nuclei in the early Universe and heavy nuclei in the collapse or merger of compact astrophysical objects, and affects the neutrino signal from a future galactic supernova. Astrophysical neutrinos are usually studied through so-called quantum kinetic equations (QKEs), which are evolution equations for the one-body reduced neutrino density matrix, accounting for both momentum and flavor degrees of freedom [1–5]. The QKEs have been derived from quantum field theory using various methods, including the two-particle-irreducible (2PI) effective action [6] truncated to three loops [3,7]. The QKEs involve both coherent forward scattering and collisional kernel and lead to a rich phenomenology of collective phenomena and flavor instabilities (see the review [8] and references therein).

While the computational implementation of the full QKEs and their interface with compact objects evolution codes is an arduous task, understanding the limits of applicability of the one-body approach underlying the QKEs remains an active area of research. The question whether the one-body analysis leaves out important many-body correlations and entanglement effects goes back to the early days of the field [9,10] and has received attention over the years [11–16].

More recently, the validity of the QKE treatment of the neutrino gas has come under scrutiny in the context of quantum many-body approaches to this problem (see [17] and references therein). As far as we are aware, all existing quantum many-body studies of the neutrino system use a truncated Hamiltonian $H_{\nu\nu}^{(T)}$ [18] that only couples pairs of momentum-space neutrino operators satisfying forward kinematics. In other words, $H_{\nu\nu}^{(T)}$ contains terms that either preserve or exchange the momenta of interacting neutrino pairs (forward and exchange terms). As argued in Ref. [19], the use of the truncated Hamiltonian is not justified in a first-principles many-body approach. On the other hand, the truncated ν-ν Hamiltonian has the virtue of mapping onto a spin-spin Hamiltonian with all-to-all couplings [18], which is amenable to many-body analyses [20–31] and implementation on quantum computers [32–36]. In certain regimes, the many-body results are at variance with the QKE expectations (see for example Refs. [17,29,30]), and there is an ongoing debate on whether these calculations can indeed challenge the validity of the QKEs' approach [19,37,38].

The path towards more realistic many-body studies requires several developments, which include: (i) assessing the impact of using the full many-body Hamiltonian rather than its truncated version, (ii) exploring more general initial pure states (not product states of plane waves), and possibly admixtures of pure states, that more realistically describe the physical system, and (iii) studying the dynamics of larger systems and systematically studying the scaling of relevant observables with the number of neutrinos, including neutrino interactions with other particles. In this work,

we address point (i) above: first, we work out the full neutrino-neutrino Hamiltonian $H_{\nu\nu}$ and set up the framework to implement the time evolution using the occupation number representation. Then we explore the evolution of simple initial states. In this simplified setting, we study the time scales for evolution of flavor and momentum degrees of freedom and their interplay. While we use a plane wave single-particle basis, we emphasize that, in principle, any initial state can be built within this formalism, thus allowing one to study point (ii) above.

This paper is organized as follows: in Sec. II we set up the basic formalism, present the full Hamiltonian and give its matrix elements in the occupation number basis. In Sec. III we introduce the one-body density matrix and the corresponding entanglement entropy, emphasizing the interplay between flavor and momentum degrees of freedom. In Sec. IV we discuss the relevant energy scales in the problems of astrophysical interest. In Sec. V we study the time evolution in a toy model with $N = 2$, illustrating some features that generalize to larger systems. In Sec. VI we study the time evolution of neutrino systems with $N = 6, 8, 10$ in a two-dimensional setup and investigate qualitative and quantitative differences that emerge when using the full and truncated Hamiltonian. We summarize our results in Sec. VII and provide some more technical details in Appendixes A and B.

II. FORMALISM

In order to write down the Hamiltonian we describe neutrino fields $\nu_\alpha(x)$ as four-component spinors ($\alpha \in \{e, \mu, \tau\}$ denoting the flavor). At energies much smaller than the electroweak scale the Hamiltonian takes the form (repeated flavor indices are summed over)

$$H = H_{\rm kin} + H_{\nu\nu} + H_{\nu-m} \tag{1}$$

with

$$\begin{aligned} H_{\rm kin} &= \int d^3x\, \bar\nu_\alpha(x)(-i\delta_{\alpha\beta}\boldsymbol{\gamma}\cdot\boldsymbol{\nabla} + m_{\alpha\beta})\nu_\beta(x), \\ H_{\nu\nu} &= \frac{G_F}{\sqrt{2}}\int d^3x\, \bar\nu_\alpha(x)\gamma_\mu P_L \nu_\alpha(x)\bar\nu_\beta(x)\gamma^\mu P_L \nu_\beta(x), \end{aligned} \tag{2}$$

where we will use the following gamma matrices:

$$\begin{aligned} &\gamma^0 = \begin{pmatrix} 0 & \sigma^0 \\ \sigma^0 & 0 \end{pmatrix}, \qquad \gamma^i = \begin{pmatrix} 0 & \sigma^i \\ -\sigma^i & 0 \end{pmatrix} \\ &\gamma_5 = i\gamma^0\gamma^1\gamma^2\gamma^3 \end{aligned} \tag{3}$$

with σ^0 being the two-dimensional identity matrix and σ^i the ith Pauli matrix. $P_L = (1-\gamma_5)/2$, and m is a complex mass matrix for Dirac neutrinos (for Majorana neutrino the kinetic term acquires an overall factor of $1/2$ and the mass matrix becomes symmetric). $H_{\nu-m}$ denotes the interaction of neutrinos with quarks and charged leptons. For a complete description of neutrino-matter interaction see, for example, [7]. In this work we do not consider the effects of $H_{\nu-m}$. In what follows we expand the neutrino fields in creation and annihilation operators and derive a representation of the Hamiltonian in Fock space.

A. Neutrino fields and spinors

We expand the free Dirac neutrino fields as follows:

$$\begin{aligned} \nu_i(x) = \sum_{h=\pm}\int \frac{d^3\mathbf{p}}{(2\pi)^3}\Big(&u(\mathbf{p},h)a_i(\mathbf{p},h)e^{-ipx} \\ &+ v(\mathbf{p},h)b_i^\dagger(\mathbf{p},h)e^{ipx}\Big) \end{aligned} \tag{4}$$

in terms of helicity spinors $u(\mathbf{p},h)$, $v(\mathbf{p},h)$ and creation/annihilation operators for neutrinos $[a_i(\mathbf{p},h)]$ and antineutrinos $[b_i(\mathbf{p},h)]$. The $h \in \{+,-\}$ label refers to helicity and $i \in \{1,2\}$ refers to the mass eigenstate. With the normalizations adopted here, the creation and annihilation operators carry mass dimension $-3/2$ and satisfy the following anticommutation relations:

$$\{a_\alpha(\mathbf{p},h), a_\beta^\dagger(\mathbf{p}',h')\} = (2\pi)^3\delta^{(3)}(\mathbf{p}-\mathbf{p}')\delta_{hh'}\delta_{\alpha\beta}. \tag{5}$$

In our conventions the spinors are dimensionless and normalized such that

$$u^\dagger(\mathbf{p},h)u(\mathbf{p},h') = v^\dagger(\mathbf{p},h)v(\mathbf{p},h') = \delta_{hh'}. \tag{6}$$

The helicity 4-spinors are given by

$$u(\mathbf{p},+) = \sqrt{\frac{E+|\mathbf{p}|}{2E}}\begin{pmatrix} r(\mathbf{p})\xi_+(\hat{\mathbf{p}}) \\ \xi_+(\hat{\mathbf{p}}) \end{pmatrix}, \tag{7}$$

$$u(\mathbf{p},-) = \sqrt{\frac{E+|\mathbf{p}|}{2E}}\begin{pmatrix} \xi_-(\hat{\mathbf{p}}) \\ r(\mathbf{p})\xi_-(\hat{\mathbf{p}}) \end{pmatrix}, \tag{8}$$

$$v(\mathbf{p},+) = \sqrt{\frac{E+|\mathbf{p}|}{2E}}\begin{pmatrix} \xi_-(\hat{\mathbf{p}}) \\ -r(\mathbf{p})\xi_-(\hat{\mathbf{p}}) \end{pmatrix}, \tag{9}$$

$$v(\mathbf{p},-) = \sqrt{\frac{E+|\mathbf{p}|}{2E}}\begin{pmatrix} -r(\mathbf{p})\xi_+(\hat{\mathbf{p}}) \\ \xi_+(\hat{\mathbf{p}}) \end{pmatrix}, \tag{10}$$

with $E = \sqrt{\mathbf{p}^2+m^2}$ and $r(\mathbf{p}) = m/(E+|\mathbf{p}|) = \sqrt{(E-|\mathbf{p}|)/(E+|\mathbf{p}|)}$. Denoting by $\theta_{\mathbf{p}}, \phi_{\mathbf{p}}$ (the polar and azimuthal angles of $\hat{\mathbf{p}} \equiv \mathbf{p}/|\mathbf{p}|$), the helicity Pauli spinors are

$$\xi_+(\hat{\mathbf{p}}) = \begin{pmatrix} \cos\frac{\theta_\mathbf{p}}{2} \\ e^{i\phi_\mathbf{p}} \sin\frac{\theta_\mathbf{p}}{2} \end{pmatrix} \quad \xi_-(\hat{\mathbf{p}}) = \begin{pmatrix} -e^{-i\phi_\mathbf{p}} \sin\frac{\theta_\mathbf{p}}{2} \\ \cos\frac{\theta_\mathbf{p}}{2} \end{pmatrix} \tag{11}$$

and satisfy $(\vec{\sigma}\cdot\hat{\mathbf{p}})\xi_\pm(\hat{\mathbf{p}}) = \pm\xi_\pm(\hat{\mathbf{p}})$.

Throughout, we treat neutrino masses as perturbations and neglect terms of higher order in $m_i/|\mathbf{p}|$. As is well known, in this approximation the left-handed neutrino field appearing in the weak Hamiltonian only involves left-helicity neutrinos and right-helicity antineutrinos,

$$P_L\nu_i(x) = \int \frac{d^3\mathbf{p}}{(2\pi)^3}\Big(u(\mathbf{p},-)a_i(\mathbf{p},-)e^{-ipx} + v(\mathbf{p},+)b_i^\dagger(\mathbf{p},+)e^{ipx}\Big). \tag{12}$$

Further focusing on the many-body dynamics of neutrinos (ignoring antineutrinos for simplicity) we only need to consider terms involving left-helicity neutrino mode operators. To simplify the notation, we thus suppress the redundant helicity label: $a_i(\mathbf{p},-) \to a_i(\mathbf{p})$.

Finally, since the interaction Hamiltonian is most naturally expressed in terms of flavor fields, we introduce the flavor basis mode operators and express the Hamiltonian in terms of these. In the two-flavor case, the relation between mass and flavor operators is given by

$$\begin{aligned} a_e(\mathbf{p}) &= \cos\theta\, a_1(\mathbf{p}) + \sin\theta\, a_2(\mathbf{p}) \\ a_\mu(\mathbf{p}) &= -\sin\theta\, a_1(\mathbf{p}) + \cos\theta\, a_2(\mathbf{p}). \end{aligned} \tag{13}$$

B. Hamiltonian

In what follows we focus on the many-body dynamics of neutrinos, ignoring antineutrinos for simplicity. For completeness, the terms in $H_{\nu\nu}$ involving antineutrinos are reported in Appendix B. As discussed above, we quantize the fields in the mass basis and work in the ultrarelativistic limit $m_i/|\mathbf{p}| \ll 1$. We then express the Hamiltonian in terms of creation and annihilation operators of left-helicity neutrinos, for which we use the flavor basis: $a_\alpha(\mathbf{p})$, $\alpha \in \{e,\mu,\tau\}$. From now on, we restrict our discussion to the case of two flavors, e and μ. The generalization to three flavors is straightforward.

Defining $\delta m^2 = m_2^2 - m_1^2$, the kinetic term of the Hamiltonian reads

$$H_{\rm kin} = \int \frac{d\mathbf{p}}{(2\pi)^3}\left[\left(|\mathbf{p}| + \frac{m_1^2+m_2^2-\delta m^2\times\cos 2\theta}{4|\mathbf{p}|}\right)a_e^\dagger(\mathbf{p})a_e(\mathbf{p}) + \left(|\mathbf{p}| + \frac{m_1^2+m_2^2+\delta m^2\times\cos 2\theta}{4|\mathbf{p}|}\right)a_\mu^\dagger(\mathbf{p})a_\mu(\mathbf{p}) + \frac{\delta m^2\times\sin 2\theta}{4|\mathbf{p}|}\Big(a_e^\dagger(\mathbf{p})a_\mu(\mathbf{p}) + a_\mu^\dagger(\mathbf{p})a_e(\mathbf{p})\Big)\right], \tag{14}$$

with the last term representing the usual vacuum mixing term.

The neutrino-neutrino terms in the interaction Hamiltonian $H_{\nu\nu}$ take the form

$$H_{\nu\nu} = \frac{G_F}{\sqrt{2}}\sum_{\alpha,\alpha',\beta,\beta'}\int \frac{d\mathbf{q}}{(2\pi)^3}\frac{d\mathbf{q}'}{(2\pi)^3}\frac{d\mathbf{p}}{(2\pi)^3}\frac{d\mathbf{p}'}{(2\pi)^3}(2\pi)^3\delta(\mathbf{p}+\mathbf{q}-\mathbf{p}'-\mathbf{q}') \times\left(a_{\alpha'}^\dagger(\mathbf{p}')a_\alpha(\mathbf{p})a_{\beta'}^\dagger(\mathbf{q}')a_\beta(\mathbf{q})\frac{(\delta_{\alpha'\alpha}\delta_{\beta'\beta}+\delta_{\alpha'\beta}\delta_{\beta'\alpha})}{2}g(\mathbf{p}',\mathbf{p},\mathbf{q}',\mathbf{q})+\cdots\right), \tag{15}$$

with

$$g(\mathbf{p}',\mathbf{p},\mathbf{q}',\mathbf{q}) \equiv \bar{u}(\mathbf{p}',-)\gamma_\mu P_L u(\mathbf{p},-)\,\bar{u}(\mathbf{q}',-)\gamma^\mu P_L u(\mathbf{q},-) = f^\dagger(\mathbf{p}',\mathbf{q}')f(\mathbf{p},\mathbf{q}) \tag{16}$$

$$f(\mathbf{p},\mathbf{q}) = \sqrt{2}\left(e^{-i\phi_\mathbf{p}}\sin\left(\frac{\theta_\mathbf{p}}{2}\right)\cos\left(\frac{\theta_\mathbf{q}}{2}\right) - e^{-i\phi_\mathbf{q}}\cos\left(\frac{\theta_\mathbf{p}}{2}\right)\sin\left(\frac{\theta_\mathbf{q}}{2}\right)\right). \tag{17}$$

From Eq. (15) we see that $H_{\nu\nu}$ takes each pair of occupied states with momenta $\mathbf{p}$, $\mathbf{q}$ to states with momenta $\mathbf{p}'$, $\mathbf{q}'$, subject to the condition $\mathbf{p}+\mathbf{q} = \mathbf{p}'+\mathbf{q}'$, and acts on the flavors by either leaving them unchanged or by swapping them. The weight for each set of momenta considered is given by the function $g(\mathbf{p}',\mathbf{p},\mathbf{q}',\mathbf{q})$ in Eq. (16).

Note that $g(\mathbf{p}',\mathbf{p},\mathbf{q}',\mathbf{q}) = g(\mathbf{q}',\mathbf{q},\mathbf{p}',\mathbf{p}) = -g(\mathbf{p}',\mathbf{q},\mathbf{q}',\mathbf{p})$, where the last equality follows from the Fierz identities. In the forward scattering kinematics ($\mathbf{p}' = \mathbf{p}$ or $\mathbf{p}' = \mathbf{q}$), this expression reproduces the familiar factors encountered in the literature [10],

$$g(\mathbf{p},\mathbf{p},\mathbf{q},\mathbf{q}) = -g(\mathbf{q},\mathbf{p},\mathbf{p},\mathbf{q}) = 1-\hat{\mathbf{p}}\cdot\hat{\mathbf{q}}. \tag{18}$$

As an illustration, we consider the two-dimensional case with $\mathbf{p}_y = 0$ and $\mathbf{p}_x > 0$ (corresponding to $\phi_{\mathbf{p}} = 0$, $\phi_{\mathbf{q}} = 0$), which leads to

$$g(\mathbf{p}', \mathbf{p}, \mathbf{q}', \mathbf{q}) \to 2 \sin\left(\frac{\theta_{\mathbf{p}} - \theta_{\mathbf{q}}}{2}\right) \sin\left(\frac{\theta_{\mathbf{p}'} - \theta_{\mathbf{q}'}}{2}\right). \quad (19)$$

The one-dimensional case (all momenta along the z axis) corresponds to $\theta_{\mathbf{p},\mathbf{p}',\mathbf{q},\mathbf{q}'} = 0, \pi$, depending on the sign of the z-component of the momenta. Equation (19) shows that in this case a nonzero amplitude is only obtained when the initial and final state momenta are "head on" [i.e. when the momenta satisfy momentum conservation $\mathbf{p}_z + \mathbf{q}_z = \mathbf{p}'_z + \mathbf{q}'_z$ and both conditions $sign(\mathbf{q}_z) = -sign(\mathbf{p}_z)$ and $sign(\mathbf{q}'_z) = -sign(\mathbf{p}'_z)$ hold].

When working in finite volume, the formulae presented above need to be modified in the usual way. Assuming the box has linear size L and volume $V = L^3$, the 3-momenta $\mathbf{p}$ are uniquely identified by triplets of integers $(\mathbf{z}_{\mathbf{p}})_{x,y,z}$ through $(\mathbf{p})_{x,y,z} = [(2\pi)/L](\mathbf{z}_{\mathbf{p}})_{x,y,z}$. As a consequence, the integrals over 3-momenta are replaced by finite sums over triplets of integers through the usual relation,

$$\int \frac{d^3p}{(2\pi)^3} \to \frac{1}{V} \sum_{\mathbf{z}_{\mathbf{p}}}, \quad (20)$$

and the Dirac delta functions of momentum conservation become Kroeneker deltas according to

$$(2\pi)^3 \delta^{(3)}(\mathbf{p} + \mathbf{q} - \mathbf{p}' - \mathbf{q}') \to V \delta_{\mathbf{z}_p + \mathbf{z}_q - \mathbf{z}_{p'} - \mathbf{z}_{q'}, \mathbf{0}}. \quad (21)$$

C. Fock space

We consider for simplicity only two neutrino flavors (denoted by e and μ) and work in Fock space. A single-particle state is identified by the three-momentum $\mathbf{p}_i$ ($i \in \{1, \ldots, k\}$) and a flavor label α ($\alpha \in \{e, \mu\}$). We consider only neutrinos with negative helicity, so we do not have to specify any other quantum numbers. There are $2k$ single particle states and a basis vector in Fock space is specified by the set of occupation numbers $n_{i\alpha} \in \{0, 1\}$. The dimension of this space is 2^{2k}.[1]

We set out to study the problem in which the initial state has total number of neutrinos $N < k$:

$$N = \sum_{\substack{i=1,\ldots,k \\ \alpha = e,\mu}} n_{i\alpha}. \quad (22)$$

Since $H_{\nu\nu}$ conserves the total number of neutrinos, we need to evolve the state in the space of fixed N, which has dimension

$$d_{N,k} = \binom{2k}{N}. \quad (23)$$

The $d_{N,k}$ basis vectors are labeled by

$$\mathbf{n} = \{n_{1e}, n_{1\mu}, \ldots, n_{ke}, n_{k\mu}\}, \quad (24)$$

the $2k$-dimensional array of occupation numbers obeying the condition (22), and represent antisymmetrized products of N single-particle states:

$$|\mathbf{n}\rangle = \text{S.D.}\left(\prod_{i\alpha:\, n_{i\alpha}=1} |\mathbf{p}_i, \alpha\rangle\right), \quad (25)$$

where "S.D." stands for Slater determinant. A generic state is specified by $d_{N,k}$ complex amplitudes $c_{\mathbf{n}}$ as follows:

$$|\Psi\rangle = \sum_{\mathbf{n}} c_{\mathbf{n}} |\mathbf{n}\rangle. \quad (26)$$

Finally, to take into account the anticommutation of the creation and annihilation operators correctly, we need to introduce the ordering rule for the operators in defining the basis vectors $|\mathbf{n}\rangle$ in Eq. (25). The basis vectors $|\mathbf{n}\rangle$ are defined via the application of a sequence of creation operators ordered in an increasing order of flavor and momenta, i.e. momenta with a smaller label are on the left, and within a given momentum label the electron flavor goes to the left of the muon flavor. For example, the normalized basis state of three neutrinos with flavor and momenta $(\mathbf{p}_1, e), (\mathbf{p}_1, \mu), (\mathbf{p}_2, e)$ (labeled by $\mathbf{n}$ with $n_{1\mu} = n_{2e} = n_{1\mu} = 1$ and all other occupation numbers $n_{j\beta} = 0$) is given by

$$|\mathbf{n}\rangle = \frac{a_e^\dagger(\mathbf{p}_1)}{\sqrt{V}} \frac{a_\mu^\dagger(\mathbf{p}_1)}{\sqrt{V}} \frac{a_e^\dagger(\mathbf{p}_2)}{\sqrt{V}} |0\rangle. \quad (27)$$

Its complex conjugate is defined as

$$\langle \mathbf{n}| = \langle 0| \frac{a_e(\mathbf{p}_2)}{\sqrt{V}} \frac{a_\mu(\mathbf{p}_1)}{\sqrt{V}} \frac{a_e(\mathbf{p}_1)}{\sqrt{V}}. \quad (28)$$

This defines an orthonormal basis, i.e. $\langle \mathbf{n}|\mathbf{m}\rangle = \delta_{\mathbf{n},\mathbf{m}}$. The application of an annihilation operator $a_\alpha(\mathbf{p}_i)$ to a basis vector $|\mathbf{n}\rangle$ results in

$$a_\alpha(\mathbf{p}_i)|\mathbf{n}\rangle = V^{1/2} f_{\mathbf{n},i,\alpha} \delta_{n_{i,\alpha},1} |\mathbf{n}^{[i\alpha]}\rangle \quad (29)$$

where

$$\mathbf{n}^{[i\alpha]} = \mathbf{n} \quad \text{with} \quad n_{i,\alpha} \to 0 \quad (30)$$

and

[1]When considering n_f flavors, one simply makes the replacement $2k \to n_f \times k$.

$$f_{\mathbf{n},i,\alpha} = (-1)^{\sum_{(j,\beta)<(i,\alpha)} n_{j,\beta}}. \tag{31}$$

The volume factor in Eq. (29) arises due to the normalization adopted for the creation and annihilation operators [see Eq. (5) and its finite volume version]. The summation $\sum_{(j,\beta)<(i,\alpha)} n_{j,\beta}$ in the exponent of the anticommutation factor $f_{\{n\},i,\alpha}$ means that we sum $n_{j,\beta}$ for all (j,β) that are on the left of (i,α) in the ordering rule introduced above.

D. Matrix elements of the Hamiltonian

We next discuss in some detail the matrix elements of the Hamiltonian $H_{\rm Kin}$ and $H_{\nu\nu}$ in the occupation number basis. With the notation introduced in the previous subsection, the matrix element of quadratic operators of the form $a^\dagger_\alpha(\mathbf{p}_i)a_\beta(\mathbf{p}_j)$ is

$$\begin{aligned}\frac{1}{V}\langle \mathbf{m}|a^\dagger_\alpha(\mathbf{p}_i)a_\beta(\mathbf{p}_j)|\mathbf{n}\rangle &= \left(f_{\mathbf{m},i,\alpha}\,\delta_{m_{i,\alpha},1}\right)\left(f_{\mathbf{n},j,\beta}\,\delta_{n_{j,\beta},1}\right)\langle \mathbf{m}^{[i\alpha]}|\mathbf{n}^{[j\beta]}\rangle \\ &\equiv \mathcal{A}_2(\mathbf{m},\mathbf{n};\{i,\alpha\},\{j,\beta\}).\end{aligned} \tag{32}$$

The matrix elements of quartic operators of the form $a^\dagger_\alpha(\mathbf{p}_i)a^\dagger_\beta(\mathbf{p}_j)a_\epsilon(\mathbf{p}_k)a_\zeta(\mathbf{p}_l)$ are

$$\begin{aligned}\frac{1}{V^2}\langle \mathbf{m}|a^\dagger_\alpha(\mathbf{p}_i)a^\dagger_\beta(\mathbf{p}_j)a_\epsilon(\mathbf{p}_k)a_\zeta(\mathbf{p}_l)|\mathbf{n}\rangle &= (f_{\mathbf{m},i,\alpha}\delta_{m_{i,\alpha},1})(f_{\mathbf{m}^{[i\alpha]},j,\beta}\delta_{(\mathbf{m}^{[i\alpha]})_{j,\beta},1})(f_{\mathbf{n}^{[l\zeta]},k,\epsilon}\delta_{(\mathbf{n}^{[l\zeta]})_{k,\epsilon},1})(f_{\mathbf{n},l,\zeta}\delta_{n_{l,\zeta},1})\langle \mathbf{m}^{[i\alpha][j\beta]}|\mathbf{n}^{[l\zeta][k\epsilon]}\rangle \\ &\equiv \mathcal{A}_4(\mathbf{m},\mathbf{n};\{i,\alpha\},\{j,\beta\},\{k,\epsilon\},\{l,\zeta\}),\end{aligned} \tag{33}$$

where

$$\mathbf{n}^{[i\alpha][j\beta]} = \mathbf{n}^{[i\alpha]} \quad \text{with} \quad n_{j,\beta} \to 0. \tag{34}$$

With Eqs. (32) and (33), the Hamiltonian's matrix elements can be written in the following way. First, the kinetic energy, including the vacuum mixing terms, reads

$$\begin{aligned}\langle \mathbf{m}|H_{\rm Kin}|\mathbf{n}\rangle = \sum_i \Bigg[&\left(|\mathbf{p}_i| + \frac{m_1^2 + m_2^2 - \delta m^2 \times \cos 2\theta}{4|\mathbf{p}_i|}\right)\mathcal{A}_2(\mathbf{m},\mathbf{n};\{i,e\},\{i,e\}) \\ &+ \left(|\mathbf{p}_i| + \frac{m_1^2 + m_2^2 + \delta m^2 \times \cos 2\theta}{4|\mathbf{p}_i|}\right)\mathcal{A}_2(\mathbf{m},\mathbf{n};\{i,\mu\},\{i,\mu\}) \\ &+ \frac{\delta m^2 \times \sin 2\theta}{4|\mathbf{p}_i|}\Big(\mathcal{A}_2(\mathbf{m},\mathbf{n};\{i,e\},\{i,\mu\}) + \mathcal{A}_2(\mathbf{m},\mathbf{n};\{i,\mu\},\{i,e\})\Big)\Bigg].\end{aligned} \tag{35}$$

The matrix elements of the normal-ordered interaction Hamiltonian can be written using Eq. (33). For the full Hamiltonian including nonforward terms, one finds

$$\begin{aligned}\langle \mathbf{m}|H^{(F)}_{\nu\nu}|\mathbf{n}\rangle = &-\frac{1}{V}\frac{G_F}{2\sqrt{2}}\sum_{\alpha,\beta=e,\mu}\sum_{i,j,k,l}\delta_{\mathbf{z}_{p_i}+\mathbf{z}_{p_j}-\mathbf{z}_{p_k}-\mathbf{z}_{p_l},\mathbf{0}}\,g(\mathbf{p}_i,\mathbf{p}_k,\mathbf{p}_j,\mathbf{p}_l) \\ &\times\Big[\mathcal{A}_4(\mathbf{m},\mathbf{n};\{i,\alpha\},\{j,\beta\},\{k,\alpha\},\{l,\beta\}) + \mathcal{A}_4(\mathbf{m},\mathbf{n};\{i,\alpha\},\{j,\beta\},\{k,\beta\},\{l,\alpha\})\Big].\end{aligned} \tag{36}$$

Finally, restricting summation over k, l in Eq. (36) to the forward limit ($k = i$ or $l = i$), we obtain the usual truncated ("forward scattering") Hamiltonian,

$$\langle \mathbf{m}|H^{(T)}_{\nu\nu}|\mathbf{n}\rangle = -\frac{1}{V}\frac{G_F}{\sqrt{2}}\sum_{\alpha,\beta=e,\mu}\sum_{i,j}(1-\hat{\mathbf{p}}_i\cdot\hat{\mathbf{p}}_j)\Big[\mathcal{A}_4(\mathbf{m},\mathbf{n};\{i,\alpha\},\{j,\beta\},\{i,\alpha\},\{j,\beta\}) + \mathcal{A}_4(\mathbf{m},\mathbf{n};\{i,\alpha\},\{j,\beta\},\{i,\beta\},\{j,\alpha\})\Big] \tag{37}$$

where the summations of i, j run over all momentum modes.

III. REDUCED DENSITY MATRICES AND ENTANGLEMENT ENTROPY

The full many-body system described by the state $|\Psi\rangle$ in Eq. (26) can be partitioned into two subsystems in various ways, and the corresponding entanglement can be studied. In this context, the key object is the reduced density matrix, obtained by tracing over one of the two subsystems, starting from the full description of the state given by the density operator

$$\rho = |\Psi\rangle\langle\Psi| = \sum_{\mathbf{n},\mathbf{m}} c_{\mathbf{n}} c^*_{\mathbf{m}} |\mathbf{n}\rangle\langle\mathbf{m}|. \tag{38}$$

A central object in our study is the one-body reduced density matrix that corresponds to partitioning the system into one particle versus $N-1$ particles and tracing over $N-1$ particle states. This object is of great interest because (i) neutrino measurements involve interactions of single neutrinos, hence knowledge of the one-body density matrix allows one to predict all observables of interest; (ii) the von Neumann entropy computed in terms of the one-body density matrix quantifies the degree of entanglement of a single neutrino with the other $N-1$; and (iii) the QKEs are evolution equations for the one-body reduced density matrix. Therefore, the one-body reduced density matrix provides the common ground on which one can study and compare QKEs and many-body approaches.

Denoting the single-particle states by $|\psi_i\rangle = |\mathbf{p}_{k_i}, \alpha_{f_i}\rangle$ (with $\alpha_{f_i} \in \{e, \mu\}$), using the notation introduced in Sec. II C the one-body reduced density matrix takes the form

$$\rho^{(1)} = \sum_{i,j} |\psi_i\rangle\langle\psi_j| \rho^{(1)}_{ij}, \tag{39}$$

$$\rho^{(1)}_{ij} = \frac{1}{N} \sum_{\mathbf{n},\mathbf{m}} c_{\mathbf{n}} c^*_{\mathbf{m}} \delta_{n_i 1} \delta_{m_j 1} f_{\mathbf{n},i} f_{\mathbf{m},j} \delta_{\mathbf{n}^{[i]},\mathbf{m}^{[j]}}. \tag{40}$$

An alternative and very useful expression for the elements of the one-body reduced density matrix in terms of expectation values of creation and annihilation operators of single-particle states is given by

$$\rho^{(1)}_{ij} = \frac{1}{N} \langle\Psi| \frac{a^\dagger_j}{\sqrt{V}} \frac{a_i}{\sqrt{V}} |\Psi\rangle. \tag{41}$$

The von Neumann entropy computed with $\rho^{(1)}$,

$$S(\rho^{(1)}) = -\mathrm{Tr}(\rho^{(1)} \log \rho^{(1)}), \tag{42}$$

provides a measure of the entanglement between a single particle and the rest of the system [39].

Invariance under translations and orthogonality of single-particle momentum eigenstates implies that $\rho^{(1)}$ has a block structure on orthogonal single-particle subspaces labeled by three-momentum:

$$\rho^{(1)} = \sum_{i=1}^{k} \sum_{\alpha,\beta \in \{e,\mu\}} |\mathbf{p}_i, \alpha\rangle\langle\mathbf{p}_i, \beta| \rho^{(1)}_{\alpha\beta}(\mathbf{p}_i), \tag{43}$$

$$\rho^{(1)}_{\alpha\beta}(\mathbf{p}) = \frac{1}{N} \langle\Psi| \frac{a^\dagger_\beta(\mathbf{p})}{\sqrt{V}} \frac{a_\alpha(\mathbf{p})}{\sqrt{V}} |\Psi\rangle. \tag{44}$$

Up to a normalization, $\rho^{(1)}_{\alpha\beta}(\mathbf{p})$ is the dynamical quantity appearing in the QKEs. The diagonal entries are positive definite and represent the occupation numbers of electron and muon neutrinos in momentum $\mathbf{p}$, normalized to N. For each momentum $\mathbf{p}_i$, it is convenient to define

$$N^\pm_i = \rho^{(1)}_{ee}(\mathbf{p}_i) \pm \rho^{(1)}_{\mu\mu}(\mathbf{p}_i). \tag{45}$$

N^+_i is the total occupation number in momentum $\mathbf{p}_i$ (normalized to N), and it is very useful to study the kinetic properties of the state. On the other hand, N^-_i characterizes the flavor content of the state in momentum $\mathbf{p}_i$. In what follows, among other things, we will use the time dependence of $N^\pm_i$ to identify the time scales of flavor and kinetic evolution.

Note that $\rho^{(1)}_{\alpha\beta}(\mathbf{p}_i)$ is not a density matrix: its trace over flavor indices is N^+_i/N, where N^+_i is the total occupation number of momentum bin $\mathbf{p}_i$, irrespective of flavor [see Eq. (45)]. When $N^+_i \neq 0$, rescaling by N^+_i/N, we can define density matrices in flavor space for each momentum bin,

$$\bar{\rho}^{(i)} = \sum_{\alpha,\beta \in \{e,\mu\}} |\mathbf{p}_i, \alpha\rangle\langle\mathbf{p}_i, \beta| \bar{\rho}^{(i)}_{\alpha\beta}(\mathbf{p}_i), \tag{46}$$

$$\bar{\rho}^{(i)}_{\alpha\beta}(\mathbf{p}_i) = \frac{N}{N^+_i} \rho^{(1)}_{\alpha\beta}(\mathbf{p}), \tag{47}$$

in terms of which the full one-body density matrix reads[2]:

$$\rho^{(1)} = \sum_{i=1}^{k} \frac{N^+_i}{N} \bar{\rho}^{(i)}. \tag{48}$$

Finally, the von Neumann entropy of $\rho^{(1)}$ can be written as

$$S(\rho^{(1)}) = -\sum_i \frac{N^+_i}{N} \log \frac{N^+_i}{N} + \sum_i \frac{N^+_i}{N} S(\bar{\rho}^{(i)}). \tag{49}$$

This expression shows that the entanglement entropy of a single neutrino with the rest of the system can arise from

[2]Note that when $N^+_i \to 0$, all entries of $\rho^{(i)}_{\alpha\beta}(\mathbf{p}_i)$ vanish, so that there is no singularity in the definition of $\bar{\rho}^{(i)}$. Moreover, in the limit $N^+_i \to 0$ one also has $N^+_i \bar{\rho}^{(i)} \to 0$, hence no contribution to $\rho^{(1)}$ from momentum bin $\mathbf{p}_i$.

entanglement in both momentum (first term above) and flavor (second term above).

To make the above statements more precise, we can further trace the one-body density matrix over flavor or momentum degrees of freedom. Tracing over flavor, we get

$$\rho^{(1),K} = \sum_{i=1}^{k} \frac{N_i^+}{N} |\mathbf{p}_i\rangle\langle\mathbf{p}_i|, \tag{50}$$

$$S(\rho^{(1),K}) = -\sum_i \frac{N_i^+}{N} \log \frac{N_i^+}{N}. \tag{51}$$

Similarly, tracing over momenta gives

$$\rho_{\alpha\beta}^{(1),F} = \sum_{i=1}^{k} \rho_{\alpha\beta}^{(1)}(\mathbf{p}_i), \tag{52}$$

with $\rho_{\alpha\beta}^{(1)}(\mathbf{p}_i)$ defined in Eq. (44). For an initial state containing N_e electron neutrinos and N_μ muon neutrinos across all momentum modes, one finds $\rho^{(1),F} = \mathrm{diag}(N_e/N, N_\mu/N)$.

The time over which $S(\rho^{(1)})$, $S(\rho^{(1),K})$, $S(\rho^{(1),F})$, $S(\bar{\rho}^{(i)})$ reach the first maximum are proxy timescales for global, kinetic, and flavor equilibration. We will illustrate these points in Sec. VI.

IV. SETUP FOR HOT AND DENSE MEDIA

In this section, we discuss the energy scales characterizing the dynamics of neutrinos in situations of astrophysical interest and define a rescaled dimensionless Hamiltonian suitable for computational implementation. In situations of astrophysical interest, such as just below the decoupling region in a supernova, the initial state of the neutrinos is not too far from equilibrium. Therefore, it makes sense to introduce a notion of near-equilibrium distribution and temperature, which characterizes the typical scale of the neutrino's momenta. In equilibrium, N, T, and V are related by $N/V = (3\zeta(3)T^3)/(4\pi^2)$. In our near-equilibrium situation, we assume that the above relation is approximately valid and assume the scaling $1/V \sim T^3/N$ to estimate the relative size of the various contributions to the Hamiltonian.[3]

When the temperature of the system is order MeV, widely separated energy scales enter the Hamiltonian, that is,

$$|\mathbf{p}| \sim T \gg G_F T^3 \gg \delta m^2/T. \tag{53}$$

The scales T and $G_F T^3$ differ by about 10 orders of magnitude. As discussed below, this wide separation effectively removes the effect of self-interactions connecting neutrino pairs with different kinetic energy, i.e. with $|\mathbf{p}_i| + |\mathbf{p}_j| \neq |\mathbf{p}_i'| + |\mathbf{p}_j'|$. On the other hand, $G_F T^3$ and $\delta m^2/T$ differ by 2 to 3 orders of magnitude depending on the magnitude of the mass splitting used. These two scales together control the flavor evolution of the system.

To make the interplay between the three parameters more explicit, we rescale the Hamiltonian for the rest of the discussion. We take as the unit of energy (and inverse time) the quantity $\mathcal{E} \equiv G_F/(\sqrt{2}V)$ and introduce the dimensionless parameters,

$$\bar{T} = \frac{T}{\mathcal{E}} \sim 10^{10} \tag{54}$$

$$\bar{\omega} = \frac{\delta m^2}{4T\mathcal{E}} \sim 10^{-3} - 10^{-2} \tag{55}$$

$$|\tilde{\mathbf{p}}| = \frac{|\mathbf{p}|}{T} \sim O(1). \tag{56}$$

The Hamiltonian of the neutrinos can now be written in terms of dimensionless operators in the following way:

$$\begin{aligned} H^{(F/T)} &= \mathcal{E}(\bar{H}_{\mathrm{Kin}} + \bar{H}_{\nu\nu}^{(F/T)}) \\ \bar{H}_{\mathrm{Kin}} &= \frac{1}{V}\sum_{i=1}^{k} \left(\bar{T}|\tilde{\mathbf{p}}_i| - \frac{\bar{\omega}\cos 2\theta}{|\tilde{\mathbf{p}}_i|}\right) a_e^\dagger(\mathbf{p}_i) a_e(\mathbf{p}_i) + \left(\bar{T}|\tilde{\mathbf{p}}_i| + \frac{\bar{\omega}\cos 2\theta}{|\tilde{\mathbf{p}}_i|}\right) a_\mu^\dagger(\mathbf{p}_i) a_\mu(\mathbf{p}_i) \\ &\quad + \frac{\bar{\omega}\sin 2\theta}{|\tilde{\mathbf{p}}_i|}[a_e^\dagger(\mathbf{p}_i) a_\mu(\mathbf{p}_i) + a_\mu^\dagger(\mathbf{p}_i) a_e(\mathbf{p}_i)] \\ \bar{H}_{\nu\nu}^{(F/T)} &= -\frac{1}{V^2}\sum_{(i,j,k,l)} g(\mathbf{p}_i, \mathbf{p}_k, \mathbf{p}_j, \mathbf{p}_l) a_\alpha^\dagger(\mathbf{p}_i) a_\beta^\dagger(\mathbf{p}_j) a_\alpha(\mathbf{p}_k) a_\beta(\mathbf{p}_l). \end{aligned} \tag{57}$$

[3]For a temperature of 1 MeV, we obtain $V \sim 10^8 N$ fm^3.

Note that we have dropped the terms proportional to $(m_1^2 + m_2^2)/|\mathbf{p}_i|$ in the diagonal part of the vacuum term $\bar{H}_{\rm Kin}$, as they are always subleading compared to the term proportional to $|\mathbf{p}_i| \to \bar{T}|\tilde{\mathbf{p}}_i|$. The summation (i,j,k,l) in $\bar{H}_{\nu\nu}$ denotes all pairs that conserve 3-momentum for the full Hamiltonian $H^{(F)}$. In the truncated case $\bar{H}^{(T)}_{\nu\nu}$, we additionally impose that $\mathbf{p}_i = \mathbf{p}_k$ and $\mathbf{p}_j = \mathbf{p}_l$, or $\mathbf{p}_i = \mathbf{p}_l$ and $\mathbf{p}_j = \mathbf{p}_k$.

V. A TOY PROBLEM WITH $N = 2$

In this section, we explore the impact of the nonforward interaction on the evolution of flavor and momentum degrees of freedom in a dense neutrino system by inspecting a toy model. In the model, there are four momentum modes ($k = 4$) for neutrinos to fill, and we consider states with two neutrinos ($N = 2$). Therefore the dimension of the relevant Hilbert space is $d_{2,4} = 28$. The momentum modes $\tilde{\mathbf{p}} = \mathbf{p}/T$ in this toy system are chosen as follows:

$$\begin{aligned}
\tilde{\mathbf{p}}_1 &= (\sin\phi, \cos\phi, 0)\\
\tilde{\mathbf{p}}_2 &= \left(\sqrt{r^2 - \cos^2\phi}, -\cos\phi, 0\right)\\
\tilde{\mathbf{p}}_3 &= \left(\sin\phi, -\cos\phi - \varepsilon, 0\right)\\
\tilde{\mathbf{p}}_4 &= \left(\sqrt{r^2 - \cos^2\phi}, \cos\phi + \varepsilon, 0\right),
\end{aligned} \tag{58}$$

with $\phi \in [0, \pi/2]$, $r > 1$ and $\varepsilon \in \mathbb{R}$. In this system, $\mathbf{p}_1 + \mathbf{p}_2 = \mathbf{p}_3 + \mathbf{p}_4$ for any r, ϕ and ε. Therefore the quartic terms in $\bar{H}_{\nu\nu}$ involving creation of $\mathbf{p}_1$, $\mathbf{p}_2$ ($\mathbf{p}_3$, $\mathbf{p}_4$) and annihilation of $\mathbf{p}_3$, $\mathbf{p}_4$ ($\mathbf{p}_1$, $\mathbf{p}_2$) will have nonzero matrix elements. Note also that $|\mathbf{p}_1| + |\mathbf{p}_2| = |\mathbf{p}_3| + |\mathbf{p}_4|$ only when $\varepsilon = 0$. One important finding in this section is that the nonforward interaction significantly affects the time evolution only when $\varepsilon \lesssim 1/\bar{T}$, i.e. when the difference in kinetic energy of the two pairs is on the order of or smaller than potential energy due to the self-interactions.

The Hamiltonian is block diagonal in the basis of Eq. (25) since it commutes with the total momentum operator and hence connects states with the same total momentum. Among the 28 basis states, 4 states have two neutrinos with the same momentum and different flavor. These 4 states have total momentum of $2\mathbf{p}_i$, and they each form a 1×1 block. Second, for the blocks with a total momentum of $\mathbf{p}_i + \mathbf{p}_j$ ($i \neq j$), there are 4 such states in each block due to the choice of flavor for each neutrino. Therefore there are six 4×4 blocks with those total momenta. Finally, since $\mathbf{p}_1 + \mathbf{p}_2 = \mathbf{p}_3 + \mathbf{p}_4$, blocks with total momenta $\mathbf{p}_1 + \mathbf{p}_2$ and $\mathbf{p}_3 + \mathbf{p}_4$ are connected via $\bar{H}_{\nu\nu}$ for the full Hamiltonian. In summary, for the only-forward Hamiltonian, there are four 1×1 blocks and six 4×4 blocks, while for the full Hamiltonian, there are four 1×1 blocks, four 4×4 blocks, and one 8×8 block connecting states with $\mathbf{p}_1 + \mathbf{p}_2$ and $\mathbf{p}_3 + \mathbf{p}_4$.

Let us take a closer look at the 8×8 block. We order the eight basis vectors $|v_1\rangle \ldots |v_8\rangle$ as follows:

$$\begin{aligned}
V|v_1\rangle &= a_e^\dagger(\mathbf{p}_1)a_e^\dagger(\mathbf{p}_2)|0\rangle, & V|v_5\rangle &= a_e^\dagger(\mathbf{p}_3)a_e^\dagger(\mathbf{p}_4)|0\rangle\\
V|v_2\rangle &= a_e^\dagger(\mathbf{p}_1)a_\mu^\dagger(\mathbf{p}_2)|0\rangle, & V|v_6\rangle &= a_e^\dagger(\mathbf{p}_3)a_\mu^\dagger(\mathbf{p}_4)|0\rangle\\
V|v_3\rangle &= a_\mu^\dagger(\mathbf{p}_1)a_e^\dagger(\mathbf{p}_2)|0\rangle, & V|v_7\rangle &= a_\mu^\dagger(\mathbf{p}_3)a_e^\dagger(\mathbf{p}_4)|0\rangle\\
V|v_4\rangle &= a_\mu^\dagger(\mathbf{p}_1)a_\mu^\dagger(\mathbf{p}_2)|0\rangle, & V|v_8\rangle &= a_\mu^\dagger(\mathbf{p}_3)a_\mu^\dagger(\mathbf{p}_4)|0\rangle.
\end{aligned}$$

To write down the matrix elements of the Hamiltonian in these basis states, we first introduce shorthand notations:

$$D_{ij}(\pm_i, \pm_j) = \bar{T}(|\tilde{\mathbf{p}}_i| + |\tilde{\mathbf{p}}_j|) \pm_i \frac{\bar{\omega}\cos 2\theta}{|\tilde{\mathbf{p}}_i|} \pm_j \frac{\bar{\omega}\cos 2\theta}{|\tilde{\mathbf{p}}_j|} \tag{59}$$

$$\bar{\omega}_i = \frac{\bar{\omega}\sin 2\theta}{|\tilde{\mathbf{p}}_i|} \tag{60}$$

for the kinetic parts and

$$f_{ij} = f(\mathbf{p}_i, \mathbf{p}_j) \tag{61}$$

$$M = \begin{pmatrix} 4 & 0 & 0 & 0\\ 0 & 2 & 2 & 0\\ 0 & 2 & 2 & 0\\ 0 & 0 & 0 & 4 \end{pmatrix} \tag{62}$$

for the interactions, with the function $f(\mathbf{p}_i, \mathbf{p}_i)$ in Eq. (61) defined in Eq. (17). With these notations, the kinetic part of the Hamiltonian, $\bar{H}_{\rm Kin}$, including vacuum mixing, takes the form

$$\bar{H}_{\rm Kin} = \begin{pmatrix}
D_{12}(-,-) & \bar{\omega}_2 & \bar{\omega}_1 & 0 & 0 & 0 & 0 & 0\\
\bar{\omega}_2 & D_{12}(-,+) & 0 & \bar{\omega}_1 & 0 & 0 & 0 & 0\\
\bar{\omega}_1 & 0 & D_{12}(+,-) & \bar{\omega}_2 & 0 & 0 & 0 & 0\\
0 & \bar{\omega}_1 & \bar{\omega}_2 & D_{12}(+,+) & 0 & 0 & 0 & 0\\
0 & 0 & 0 & 0 & D_{34}(-,-) & \bar{\omega}_4 & \bar{\omega}_3 & 0\\
0 & 0 & 0 & 0 & \bar{\omega}_4 & D_{34}(-,+) & 0 & \bar{\omega}_3\\
0 & 0 & 0 & 0 & \bar{\omega}_3 & 0 & D_{34}(+,-) & \bar{\omega}_4\\
0 & 0 & 0 & 0 & 0 & \bar{\omega}_3 & \bar{\omega}_4 & D_{34}(+,+)
\end{pmatrix}. \tag{63}$$

The interaction terms read

$$\bar{H}^{(T)}_{\nu\nu} = \begin{pmatrix} f^{\dagger}_{12} f_{12} M & 0 \\ 0 & f^{\dagger}_{34} f_{34} M \end{pmatrix} \tag{64}$$

and

$$\bar{H}^{(F)}_{\nu\nu} = \begin{pmatrix} f^{\dagger}_{12} f_{12} M & f^{\dagger}_{12} f_{34} M \\ f^{\dagger}_{34} f_{12} M & f^{\dagger}_{34} f_{34} M \end{pmatrix}. \tag{65}$$

One thing to note about the eigenvalue spectrum of $\bar{H}_{\nu\nu}$ is that five of them are zero and three take the same value. (When considering the total Hamiltonian, the vacuum mixing terms in $\bar{H}_{\rm Kin}$ lift this degeneracy.) This is due to the fact that each block is given by the 4×4 matrix M multiplied by the products of two f_{ab} factors, corresponding to the incoming and outgoing momentum pairs. As a result, the first four columns of $\bar{H}_{\nu\nu}$ and the last four are linearly dependent. Together with the structure of M, this implies that the rank of the matrix $\bar{H}_{\nu\nu}$ is 3. This is a special feature seen only in 2-neutrino systems.

In contrast to the above point, there is an important general feature of the problem that emerges from the analysis of this toy model. Given that in situations of (astro)physical interest $\bar{T}/\bar{\omega} > 10^{10}$, when $|\tilde{\mathbf{p}}_1| + |\tilde{\mathbf{p}}_2|$ and $|\tilde{\mathbf{p}}_3| + |\tilde{\mathbf{p}}_4|$ differ by $O(1)$, transitions between the blocks with the total momentum of $\mathbf{p}_1 + \mathbf{p}_2$ and $\mathbf{p}_3 + \mathbf{p}_4$ caused by $H^{(F)}$ become negligible. The two blocks are dynamically decoupled, similarly to what happens in any two-level quantum system when the off-diagonal mixing term is much smaller than the unperturbed level splitting. In this regime, the evolution is effectively controlled by the truncated Hamiltonian $\bar{H}^{(T)}$. Only when the difference between $|\tilde{\mathbf{p}}_1| + |\tilde{\mathbf{p}}_2|$ and $|\tilde{\mathbf{p}}_3| + |\tilde{\mathbf{p}}_4|$ is of similar magnitude as $|f^{\dagger}_{12} f_{34}|/\bar{T}$, do the neutrino-neutrino nonforward interactions contribute to the dynamics. To test this observation, we analyze the time evolution of the toy model with $\bar{T} = 10^4$, $\bar{\omega} = 1$, and $\sin 2\theta = 0.8$ as we vary the parameter ε that controls the "kinetic energy conservation" condition through $|\tilde{\mathbf{p}}_3| + |\tilde{\mathbf{p}}_4| = |\tilde{\mathbf{p}}_1| + |\tilde{\mathbf{p}}_2| + O(\varepsilon)$. We fix the momentum parameters to be $r = 2.0$ and $\phi = \pi/4$ and study

$$|\psi(t)\rangle = \sum_{i=1}^{8} c_i(t) |v_i\rangle. \tag{66}$$

For the purpose of illustration, we show results for initial states $|\psi(0)\rangle = |v_1\rangle$ (two electron neutrinos with momentum $\mathbf{p}_1$ and $\mathbf{p}_2$) and $|\psi(0)\rangle = |v_2\rangle$ (electron neutrino with momentum $\mathbf{p}_1$ and muon neutrino with momentum $\mathbf{p}_2$). In Fig. 1 we plot the Loschmidt echo $|\langle\psi(0)|\psi(t)\rangle|^2$ as a function of time and compare it to the time evolution obtained with the truncated ("forward") Hamiltonian. As expected, $|\langle\psi(0)|\psi(t)\rangle|^2$ starts to significantly deviate from the truncated behavior around $\varepsilon \sim 1/\bar{T} = 10^{-4}$ and the effect of nonforward scattering increases as ε decreases. For $\varepsilon \sim 10^{-5} \sim 0.1/\bar{T}$ or smaller, the evolution becomes essentially indistinguishable from the $\varepsilon = 0$ case.

This dynamical pairwise kinetic energy conservation limits the number of relevant terms in the full Hamiltonian $H^{(F)}$. This is still much less restrictive than the forward kinematics enforced in the truncated Hamiltonian $H^{(T)}$. In fact, for each pair of momenta $\mathbf{p}$ and $\mathbf{q}$, three-momentum and kinetic energy conservation open up an infinite set of momentum pairs $\mathbf{p}'$ and $\mathbf{q}'$ (parametrized by two angles as shown in Appendix A) that contribute to the evolution, to be contrasted to just one option in forward kinematics. The pairwise kinetic energy conditions become very restrictive only if one considers a one-dimensional setup. In this case, the discussion below Eq. (19) implies that $|\mathbf{p}_z| + |\mathbf{q}_z| = |\mathbf{p}'_z| + |\mathbf{q}'_z|$ only holds if $\mathbf{p}'_z = \mathbf{p}_z$ or $\mathbf{p}'_z = \mathbf{q}_z$. In other

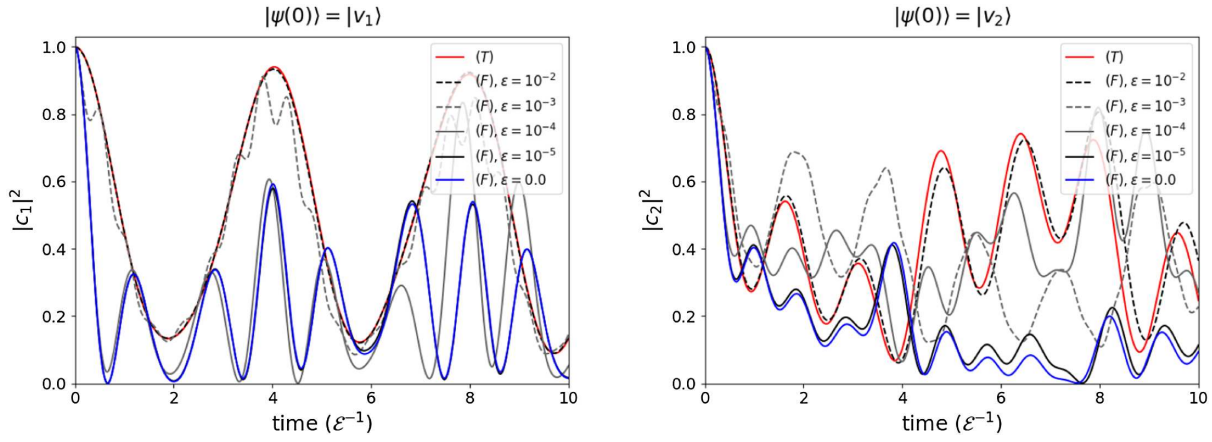

FIG. 1. Loschmidt echo $|\langle\psi(0)|\psi(t)\rangle|^2$ in the two-neutrino toy model, for $|\psi(0)\rangle = |v_1\rangle$ (left panel) and $|\psi(0)\rangle = |v_2\rangle$ (right panel). In both cases the Hamiltonian parameters are $\bar{T} = 10^4$, $\bar{\omega} = 1$, and $\sin 2\theta = 0.8$. The momentum parameters are $r = 2.0$, $\phi = \pi/4$ and $\varepsilon = 0, 10^{-2} - 10^{-5}$.

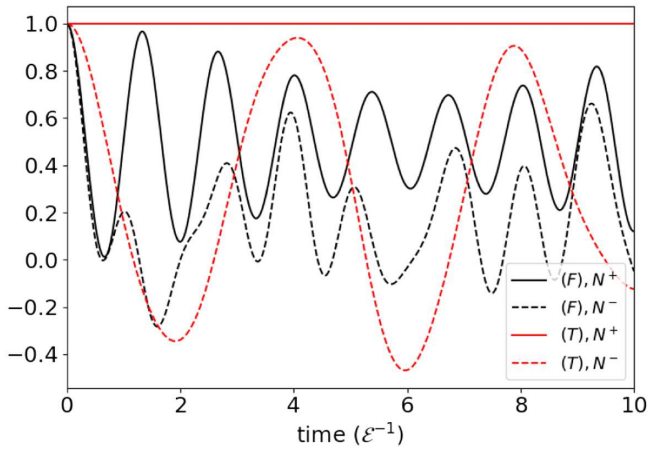

FIG. 2. Expectation values of N_1^+ and N_1^- for the mode $\mathbf{p}_1$ over time for the full and truncated Hamiltonian. The Hamiltonian parameters are chosen as $\bar{T} = 10^4$, $\bar{\omega} = 1.0$, and $\sin 2\theta = 0.8$. The momentum parameters are $r = 2.0, \phi = \pi/4$ and $\varepsilon = 0.0$. The initial state is v_1, i.e., neutrinos with flavor e and momentum $\mathbf{p}_1$, $\mathbf{p}_2$.

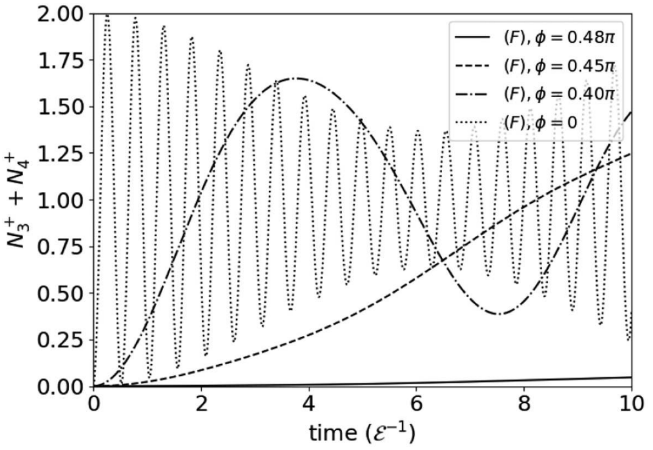

FIG. 3. Time evolution induced by the full Hamiltonian $H^{(F)}$ for the sum of occupation numbers $N_3^+ + N_4^+$ of initially unoccupied momentum modes $\mathbf{p}_3$ and $\mathbf{p}_4$ [$|\psi(0)\rangle = |v_1\rangle$]. The Hamiltonian parameters are $\bar{T} = 10^4$, $\bar{\omega} = 1$, and $\sin 2\theta = 0.8$. The momentum parameters are $r = 2.0$ and $\varepsilon = 0$ while we vary ϕ.

words, the pairwise kinetic energy condition enforces forward or exchange kinematics and the evolution with the full and truncated Hamiltonian effectively coincide.

When kinetic energy conservation holds approximately, i.e. at $\varepsilon \sim 0$, all eight states with total momentum of $\mathbf{p}_1 + \mathbf{p}_2$ (or equivalently $\mathbf{p}_3 + \mathbf{p}_4$) get nonzero amplitudes over time without suppression via $\bar{T}$. This spread of amplitude is governed by the interplay between the neutrino's self-interaction and their vacuum oscillation. One then naturally expect to see the effect of nonforward scattering in flavor equilibration and randomization of momenta. We can see a hint of this even in this two-neutrino toy model. To study these phenomena, in Fig. 2, we compare the N_1^+ and N_1^- [see definition in Eq. (45)] for the state evolved via either $H^{(F)}$ (in black) or $H^{(T)}$ (in red). Obviously, kinetic evolution occurs only with the full Hamiltonian—the occupation number of a given momentum mode cannot change via forward scattering or exchange processes. This is evident in the constant solid red line showing the total occupation number of the momentum mode. Regarding flavor conversion, which occurs for both full and truncated setups, the evolution speed at initialization appears to be faster with the full Hamiltonian. This is correlated with the fact that the total occupation of the mode decreases quickly due to the nonforward interaction. Therefore, at least in this toy model, the time scales for kinetic evolution (and ultimately thermalization) and flavor evolution are correlated. We will further investigate the relation between kinetic and flavor equilibration in the next section.

We close this section by pointing out that the evolution time scales can be affected by the angular factors $g(\mathbf{p}', \mathbf{p}, \mathbf{q}', \mathbf{q})$ in the Hamiltonian matrix elements, given in Eq. (16). From now onward, we will refer to these as the "g factors." The magnitude of the g factors depends on the relative angles of the incoming and outgoing momentum modes, parametrized in this simple model by ϕ in Eq. (58). In Fig. 3, we plot the time dependence of the sum of occupation numbers $N_3^+ + N_4^+$ of initially unoccupied momentum modes [$|\psi(0)\rangle = |v_1\rangle$] for different choices of the angle ϕ in Eq. (58). As ϕ approaches $\pi/2$, the angle between $\mathbf{p}_1$ and $\mathbf{p}_2$ decreases and the effect of nonforward scattering vanishes. This has physical implications related to geometric effects, as neutrino crossing angles away from a source are geometrically suppressed. Besides this, even in absence of geometric suppression, this feature is expected to slow down the evolution time scales in simulations with a small number of neutrinos and a small number of available momentum modes. Some of these artifacts will appear in our discussion in the next section.

In this section, we studied several key features of the full Hamiltonian in the two-neutrino toy model:

(i) Most notably, the hierarchy between the neutrino kinetic and potential energy ($\bar{T} \gg 1$) results in pairwise kinetic energy conservation. Together with three-momentum conservation, for each pair of momenta $\mathbf{p}$ and $\mathbf{q}$, this still opens up an infinite set of momentum pairs $\mathbf{p}'$ and $\mathbf{q}'$ that contribute to the evolution (see Appendix A).

(ii) Nonforward processes induce kinetic (momentum) randomization and have the potential for accelerating flavor evolution.

(iii) The quantitative impact of nonforward terms in the Hamiltonian depends on the magnitude of the g factors, which decrease as the relative angle of two incoming momentum modes decreases.

VI. TWO-DIMENSIONAL MODELS

In this section, we study the time evolution of various neutrino systems under the full Hamiltonian $H^{(F)}$ and truncated Hamiltonian $H^{(T)}$ with momentum modes taken on a two-dimensional grid:

$$\tilde{\mathbf{p}} \equiv \mathbf{p}/T = \frac{2\pi}{LT}\mathbf{z}$$
$$\mathbf{z} = \{(z_x, z_y); z_x, z_y \in \mathbb{Z}\}$$
$$\text{with} \quad 0 < |\mathbf{z}| \leq z_{\max} \quad \text{and} \quad 0 < z_x. \tag{67}$$

We exclude the zero mode and introduce a "UV" cutoff $p_{\max}$ that sets the maximal magnitude on the momenta. Moreover, we only consider the modes with a positive x component to mimic astrophysical situations in which there is a net flux of neutrinos.

With this setup, we first demonstrate that kinetic energy conserves pair-by-pair through the self-interactions and show that we can safely take this as an exact conservation law at typical temperature of interest $T \gtrsim$ MeV. Given that, we impose the pairwise kinetic energy conservation on both the Hilbert space and Hamiltonian and explore the collective flavor evolution and kinetic (momentum) randomization in this system while varying the number of neutrinos $N = 6, 8, 10$ and initial states. All codes developed for the numerical simulations performed in this section are available online.[4]

A. Pairwise kinetic energy conservation

As discussed in Sec. V, when the typical magnitude of neutrino three-momenta (dictated by the temperature) is much larger than the neutrino self-interaction potential energy, out of all couplings contained in $H_{\nu\nu}$, only the ones satisfying approximate pairwise kinetic energy conservation are expected to affect the dynamics. Here we demonstrate this within the two-dimensional models specified by the grid of momentum modes in Eq. (67). For this purpose, we simulate the time evolution numerically via exact diagonalization of the two Hamiltonians: the full Hamiltonian and the one with the kinetic energy conservation imposed in $H_{\nu\nu}$, which we denote as $H^{(K)}_{\nu\nu}$. Explicitly, $H^{(K)}_{\nu\nu}$ is

$$\bar{H}^{(K)} = \bar{H}_{\rm Kin} + \bar{H}^{(K)}_{\nu\nu}$$
$$\bar{H}^{(K)}_{\nu\nu} = -\frac{1}{V^2}\sum_{\mathbf{p}_{i,j,k,l}\in\{\mathbf{p}\}}\Big[a^\dagger_\alpha(\mathbf{p}_i)a^\dagger_\beta(\mathbf{p}_j)a_\alpha(\mathbf{p}_k)a_\beta(\mathbf{p}_l) \times \delta_{\mathbf{p}_i+\mathbf{p}_j,\mathbf{p}_k+\mathbf{p}_l}\delta_{|\mathbf{p}_i|+|\mathbf{p}_j|,|\mathbf{p}_k|+|\mathbf{p}_l|}g(\mathbf{p}_i,\mathbf{p}_k,\mathbf{p}_j,\mathbf{p}_l)\Big]. \tag{68}$$

Comparison with Eq. (57) reveals that $\bar{H}^{(T)}_{\nu\nu} \subset \bar{H}^{(K)}_{\nu\nu} \subset \bar{H}^{(F)}_{\nu\nu}$.

[4] https://github.com/yukariyamauchi/neutrinos_beyond_fwd.

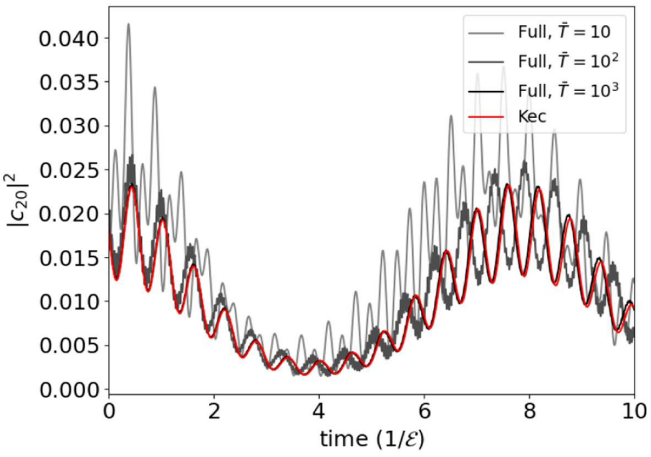

FIG. 4. The squared modulus of the amplitude of the 20th basis state simulated with $H^{(F)}$ (denoted as "Full") and with $H^{(K)}$ (denoted as "Kec"). The Hamiltonian parameters are $\bar{\omega} = 1.0$ and $\sin 2\theta = 0.8$. The model has $k = 11$ momentum modes and $N = 2$ neutrinos. Note that the black solid line is almost on top of the red solid line.

We set $z_{\max} = 3$ for the grid of momenta, which gives 11 modes. The simulation is performed in the Hilbert space with the number of neutrinos $N = 2$ and 4. Therefore the dimension of the Hilbert space is $d_{N,11} = 231$ or 7315 for $N = 2, 4$, respectively. We do not make a further truncation to the Hilbert space. In the following demonstrations, the Hamiltonian parameters are $\bar{\omega} = 1.0$ and $\sin 2\theta = 0.8$. We take as initial state at time $t = 0$ a superposition of all basis states with N electron neutrinos, assigning an equal amplitude to all such basis states:

$$|\psi(0)\rangle = \frac{1}{\sqrt{{}_{11}C_N}}\sum_{\mathbf{n}}\delta_{N,\sum_{i=1}^{11} n_{i,e}}|\mathbf{n}\rangle, \tag{69}$$

where ${}_nC_k$ denotes the binomial coefficient.

As an example, in the case of $N = 2$ the squared modulus of the amplitude of the 20th basis state, which has electron neutrinos with momentum $(z_x, z_y) = (1, -2)$ and (2,2), is shown in Fig. 4. When the temperature is low, the state can transition to other 2-neutrino states such as the one with momentum modes (1,0) and (2,0). However, as the temperature increases, such transitions are suppressed unless kinetic energy is conserved. In the infinite-temperature limit, the initial state can transition only to the states of neutrinos with momentum modes $(2, -2)$ and (1,2) on the grid. Figure 4 shows that as the temperature $\bar{T}$ goes up, $|c_{20}(t)|^2$ converges to the time evolution with $H^{(K)}$. The difference between the amplitude from $H^{(F)}$ and $H^{(K)}$ is negligible at $\bar{T} = 10^3$ (in black solid line).

To quantify more globally the difference between two simulations done with $H^{(F)}$ or $H^{(K)}$, we employ the Kullback-Leibler (KL) divergence [40], $D_{\rm KL}(P_{\rm kec}(t)||P_{\rm full}(t))$, where $P_{\rm kec}(t)$ and $P_{\rm full}(t)$ are probabilities defined by their

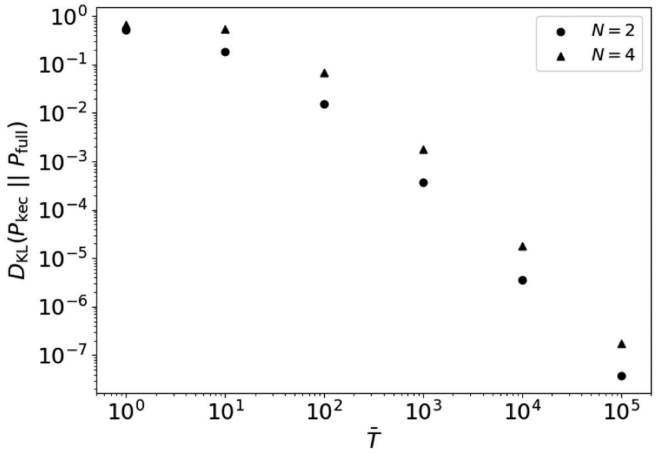

FIG. 5. The Kullback-Leibler divergence of the two probability densities $P_{\rm kec}(t = 10/\mathcal{E})$ and $P_{\rm full}(t = 10/\mathcal{E})$ defined by the set of $|c_n(t)|^2$ evolved with $H^{(K)}_{\nu\nu}$ and $H^{(F)}_{\nu\nu}$, respectively. The Hamiltonian parameters are $\bar{\omega} = 1.0$ and $\sin 2\theta = 0.8$ while varying $\bar{T}$. The model has 11 momentum modes, and the number of neutrinos is 2 or 4.

corresponding $|c_n(t)|^2$. In Fig. 5 we show the KL divergence at time $t = 10/\mathcal{E}$ for the $N = 2, 4$ systems while varying $\bar{T}$. The KL divergence decreases with temperature $\bar{T}$ according to a power law, thus offering a parametric evidence for the "dynamical" pairwise kinetic energy conservation.

B. Details of the simulated systems

In the rest of the section, we impose that pairwise kinetic energy conservation holds exactly in the neutrino-neutrino self-interaction as in $H^{(K)}$. Additionally, we exclusively focus on the neutrino self-interaction and turn off the vacuum oscillations by setting $\bar{\omega} = 0$. This condition allows us to decompose the entire Hilbert space into the subspaces with a fixed total momentum, kinetic energy, and particle numbers N_e (electron neutrino) and N_μ (muon neutrino). Even within each subspace with these fixed quantities, there are multiple disconnected subspaces—the matrix element of $H^{(F)}_{\nu\nu}$ is nonzero only when the two states have a pair of two momentum modes whose total momentum and kinetic energy are the same. On the momentum grid with $z_{\rm max} = 5$ with $k = 35$ momentum modes as shown in the left panel of Fig. 6, we focus on three such subspaces: $\mathcal{H}_1$ with $N = 6$, $\mathcal{H}_2$ with $N = 8$, and $\mathcal{H}_3$ with $N = 10$, where N denotes the total number of neutrinos. We choose the number of electron neutrinos to be $N_e = N/2 + 1$. Some defining quantities of the Hilbert spaces are summarized in Table. I.

TABLE I. Some defining quantities of the three Hilbert subspaces we study, that is, the number of neutrinos N_e, N_μ, the number of momentum modes k involved in the time evolution, total momentum, total kinetic energy, and the dimension of the Hilbert space (d_h).

Hilbert space	N_e	N_μ	k	Total $\mathbf{z}$	$\sum_i \lvert\mathbf{z}_i\rvert$	d_h
$\mathcal{H}_1$	4	2	14	(13,0)	23.30	158
$\mathcal{H}_2$	5	3	18	(16,0)	26.95	1434
$\mathcal{H}_3$	6	4	20	(21,0)	33.38	6922

The basis states in these Hilbert spaces are enumerated by picking a "reference basis state" and listing all other basis states that can be reached from the reference state via repeatedly applying the self-interaction $\bar{H}^{(K)}_{\nu\nu}$. The reference state we used for $\mathcal{H}_1$ is $|\mathbf{n}\rangle$ with

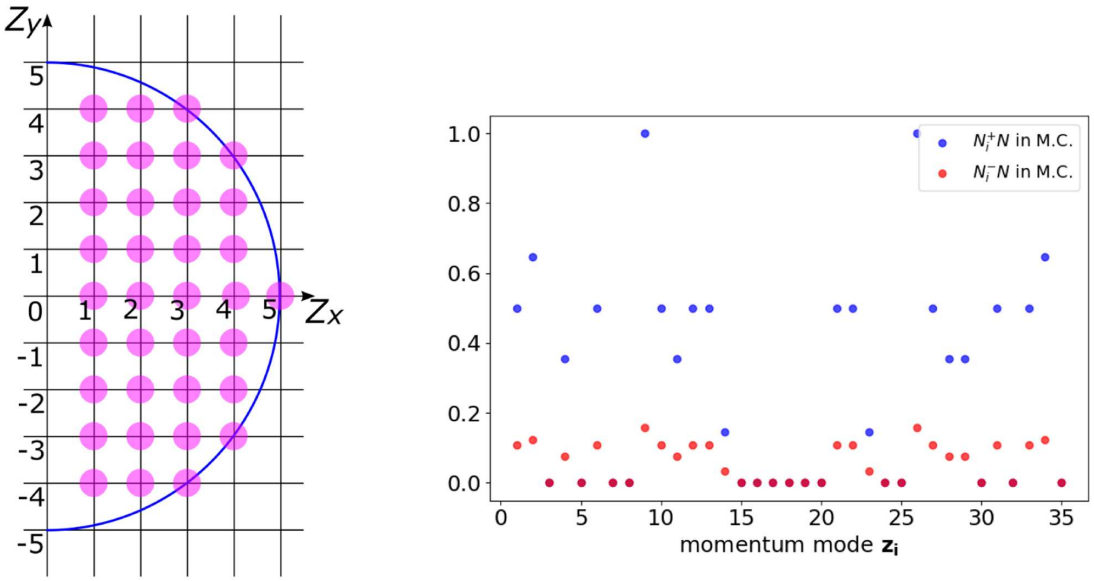

FIG. 6. Left: 35 momentum modes are shown in pink circles on the grid with the maximal magnitude $z_{\rm max} = 5$ (blue line). Right: the equilibrium expectation values of $NN_i^{+/-}$ computed with Eq. (74) are shown in blue and red, respectively, for $\mathcal{H}_3$.

$$n_{ie} = \begin{cases} 1 & i = 1, 6, 11, 26 \\ 0 & \text{otherwise} \end{cases}$$
$$n_{i\mu} = \begin{cases} 1 & i = 9, 34 \\ 0 & \text{otherwise.} \end{cases} \quad (70)$$

The reference state for $\mathcal{H}_2$ is

$$n_{ie} = \begin{cases} 1 & i = 1, 6, 11, 13, 21 \\ 0 & \text{otherwise} \end{cases}$$
$$n_{i\mu} = \begin{cases} 1 & i = 26, 29, 34 \\ 0 & \text{otherwise,} \end{cases} \quad (71)$$

and the reference state used for $\mathcal{H}_3$ is

$$n_{ie} = \begin{cases} 1 & i = 1, 6, 9, 11, 13, 21 \\ 0 & \text{otherwise} \end{cases}$$
$$n_{i\mu} = \begin{cases} 1 & i = 26, 27, 29, 34 \\ 0 & \text{otherwise.} \end{cases} \quad (72)$$

The momentum modes are labeled in an increasing order of z_y and z_x, e.g.,

$$\mathbf{z}_1 = (1, -4), \quad \mathbf{z}_6 = (3, -3), \quad \mathbf{z}_9 = (2, -2)$$
$$\mathbf{z}_{11} = (4, -2), \quad \mathbf{z}_{13} = (2, -1), \quad \mathbf{z}_{21} = (1, 1)$$
$$\mathbf{z}_{26} = (2, 2), \quad \mathbf{z}_{27} = (3, 2), \quad \mathbf{z}_{29} = (1, 3)$$
$$\mathbf{z}_{34} = (2, 4). \quad (73)$$

From these reference states, $H^{(K)}_{\nu\nu}$ populates a total of 14, 18, or 20 momentum modes for $\mathcal{H}_{1,2,3}$, thus allowing us to study the effects of nonforward scattering. The dimension of the Hilbert space becomes $d_h = 158$, 1434, and 6922 for $\mathcal{H}_{1,2,3}$, respectively.

By construction, any initial state in $\mathcal{H}_i$ ($i = 1, 2, 3$) stays in $\mathcal{H}_i$ when evolved with $H^{(K)}$. For the sake of simplicity, we study the time evolution of 15 basis states for each case. These initial states have the same momentum content as the reference states but have different flavor contents, with the total number of electron neutrinos fixed to $N/2 + 1$. For $N = 6$, there are 15 such basis states since ${}_6C_4 = 15$. For $N = 8$, 10 we picked 15 states from the ${}_8C_5$ or ${}_{10}C_6$ number of such basis states. These initial states are far from equilibrium in both flavor and kinetic degrees of freedom. We leave the study of a more realistic initial state that mimics the situation in hot dense media of neutrinos to future work.

The time evolution of these initial states is performed by exactly diagonalizing the full or truncated Hamiltonian and applying the corresponding unitary time-evolution operator e^{-iHt} to the initial state. The Hamiltonian parameters are chosen to be $\sin 2\theta = 0.8$ and $\bar{\omega} = 0$. The diagonal terms in $H_{\rm Kin}$ proportional to $\bar{T}$ are dropped since they are proportional to the identity in the restricted Hilbert spaces. For the rest of the section, we study various quantities that characterize the time evolution of the chosen initial states: Loschmidt echo, $N_i^{+/-}$, and the one-body entropies introduced in Sec. III.

We close this section by introducing a microcanonical ensemble for the systems we study [41]. All basis states of a given Hilbert space, $\mathcal{H}_i$ ($i = 1, 2, 3$), have the same kinetic energy, which dominates the energy of the basis states given the hierarchy Eq. (53). Since all the basis states $|j\rangle$ in $\mathcal{H}_i$ have the same particle numbers N_e, N_μ, and total energy, in a microcanonical ensemble they are equally probable and the corresponding density operator is

$$\rho_{\rm mc} = \frac{1}{d_h} \sum_{j=1}^{d_h} |j\rangle\langle j|. \quad (74)$$

In equilibrium, the expectation values of various observables $\mathcal{O}$ are computed as $\mathrm{Tr}[\rho_{\rm mc}\mathcal{O}]$. The equilibrium expectation values of N^+ and N^- will be used to in later sections to quantitatively assess kinetic and flavor equilibration of our models. These equilibrium values are shown in the right panel of Fig. 6 for $\mathcal{H}_3$.

C. Loschmidt echo

We begin the comparison of the time volution under the full and truncated Hamiltonian by studying the Loschmidt echo $\mathcal{L} \equiv |\langle\psi(t)|\psi(0)\rangle|^2$. At early time, the decrease of the Loschmidt echo indicates how quickly the amplitude of the wave function spreads from the initial state to the rest of the Hilbert space. The curvature of the echo at time $t = 0$ is the negative of the variance of the Hamiltonian $\langle\psi(0)|H|\psi(0)\rangle^2 - \langle\psi(0)|H^2|\psi(0)\rangle$. This variance naively quantifies how densely the initial state is connected to the rest of the Hilbert space via the Hamiltonian since the H^2 piece measures the sum of the square moduli of the Hamiltonian matrix elements between the initial state and all other states. In particular, in our simulation setup, since the initial state is taken to be one of the basis states $|\psi(0)\rangle = |i\rangle$, the curvature of the Loschmidt echo at $t = 0$ is

$$\frac{d^2}{dt^2} |\langle\psi(t)|\psi(0)\rangle|^2|_{t=0} = -\sum_{j\neq i} |\langle i|H|j\rangle|^2. \quad (75)$$

Therefore one expects that the Loschmidt echo decreases more rapidly with the full Hamiltonian than with the truncated Hamiltonian for a given initial state.

Early-time behavior of the Loschmidt echo is shown for one of 15 initial states for $N = 6$, 8, 10 in Fig. 7. As expected, the Loschmidt echo evolved under the full Hamiltonian (solid lines) decreases faster to lower values compared to those from the truncated simulation (dotted lines). Although the Loschmidt echo does not give separate

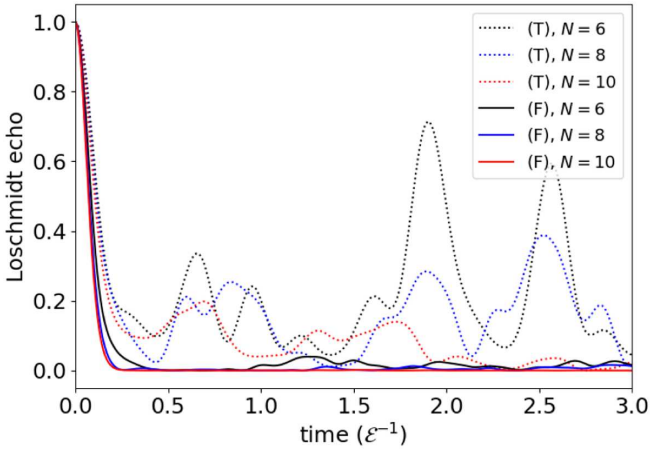

FIG. 7. Loschmidt echo over time for the three cases, $N = 6$ (in $\mathcal{H}_1$), $N = 8$ (in $\mathcal{H}_2$), and $N = 10$ (in $\mathcal{H}_3$). Results from the time evolution under the full Hamiltonian, (F), are shown in solid lines, while truncated ones, (T), are in dotted lines. For each case, we chose a basis state in $\mathcal{H}_1$, $\mathcal{H}_2$, or $\mathcal{H}_3$ as the initial state. We turn off the vacuum oscillation ($\bar{\omega} = 0$).

information about the time scale of flavor evolution or kinetic randomization, it can still provide us with the evidence that the full Hamiltonian is able to spread the amplitude of the wave function more quickly to a larger Hilbert space than what the truncated Hamiltonian can achieve. Note that the Loschmidt echo from the full simulations especially with $N = 8$ and 10 show rather quick convergence, whereas the others fluctuate about ~0.3. This is due to the smallness of the number of neutrinos and a resulting small dimension of the Hilbert space. It is demonstrated in [30] that the Loschmidt echo decreases and converges quickly for $N = 10$–16 systems under the truncated time evolution. We have confirmed this behavior in our simulations for $N = 10$–14.

To quantify the difference in randomization time scale under the full or truncated Hamiltonian, we introduce $t_{\mathcal{L}}$, defined as the time at which the Loschmidt echo reaches its first minimum. In Fig. 8, we show $t_{\mathcal{L}}$ and the Loschmidt echo at the time for all 15 initial states in all N on the left panel. The circles show $t_{\mathcal{L}}$ obtained in the wave function evolved by the full Hamiltonian, while triangles correspond to the truncated Hamiltonian. The difference between $t_{\mathcal{L}}$ and the Loschmidt echo at the time $t_{\mathcal{L}}$ by $H^{(F)}$ and $H^{(T)}$ is striking. The full time evolution, on average, achieves a minimum Loschmidt echo a few order of magnitude smaller, in a shorter time. To emphasize this point, we compare the time scale for each initial state from the full and truncated Hamiltonian on the right panel of Fig. 8. The figure shows $t_{\mathcal{L}}^{(T)} - t_{\mathcal{L}}^{(F)}$, i.e., the difference of $t_{\mathcal{L}}$ between two Hamiltonians on the horizontal axis and the ratio of the echoes $\mathcal{L}^{(T)}/\mathcal{L}^{(F)}$ on the vertical axis. For almost all initial states taken for $N = 6, 8, 10$, $t_{\mathcal{L}}$ is smaller with the full time evolution and Loschmidt echo is smaller at the first minimum. Within our study, we are not able to observe an obvious trend in $t_{\mathcal{L}}$ as we vary the number of neutrinos N. We will leave the study of the behavior of the Loschmidt echo in systems with larger N to future work.

D. Single neutrino observables

In this section we analyze kinetic randomization and flavor evolution of our neutrino systems separately through the occupation numbers N^+, N^- introduced in Eq. (45). In particular, we show that these expectation values converge to their equilibrium values from the microcanonical ensemble in Eq. (74), thus demonstrating the equilibration process of our models.

The neutrino flavor degrees of freedom evolve over time due to their vacuum oscillation (which we do not consider here by setting $\bar{\omega} = 0$) and self-interaction. While forward

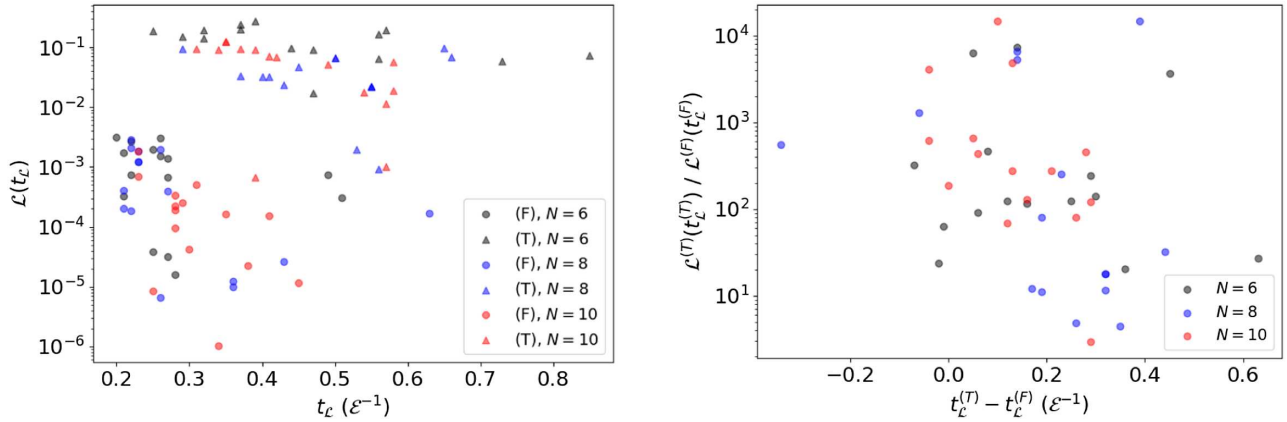

FIG. 8. Left: Loschmidt echo time scale $t_{\mathcal{L}}$ when the echo reaches its first minimum and the echo at the time. The initial states chosen in Sec. VI A are evolved either via the full and truncated Hamiltonian. These initial states differ only by the flavor content of each momentum mode, but the populated momentum modes and total number of electron (and muon) neutrinos are fixed. Due to this choice, combined with the artifact of the momentum grid, some simulations yield the same Loschmidt echo. Right: the difference between $t_{\mathcal{L}}$ and ratio of the Loschmidt echo at $t_{\mathcal{L}}$ are shown for each initial state.

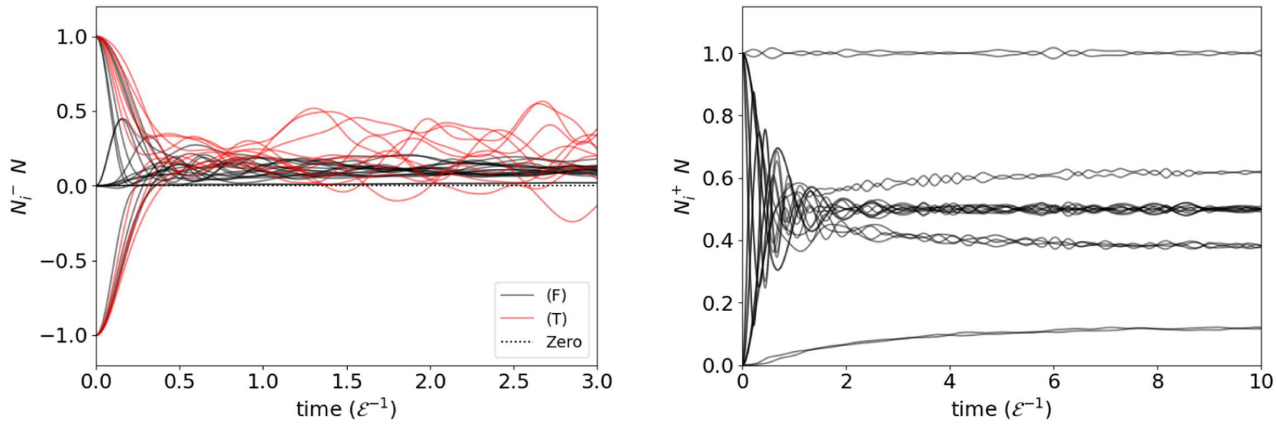

FIG. 9. Left: N_i^- (normalized to 1) for each momentum mode $\mathbf{p}_i$ over time. The initial state is a basis state in $\mathcal{H}_3$ (with $N = 10$) and is time evolved under the full (F) or truncated (T) Hamiltonian. Right: N_i^+ (normalized to 1) for each momentum mode $\mathbf{p}_i$ over time from the same simulation as the left panel.

scattering can cause flavor equilibration by exchanging flavors among neutrinos [30], nonforward scattering processes are expected to speedup the equilibration process by activating the modes which are inaccessible via forward scattering and letting flavor mixing happen within those modes. To visualize this effect, we inspect N_i^-, which is the difference between the occupation number of flavors e and μ for the momentum mode $\mathbf{z}_i$. As an example, in the left panel of Fig. 9 we show N_i^- over time for all modes $\mathbf{z}_i$ from the time evolution of a basis state in $\mathcal{H}_3$ ($N = 10$). When using the truncated Hamiltonian, only the ten initially populated bins evolve (shown in red), starting at either $NN_i^- = 1$ (electron neutrino) or $NN_i^- = -1$ (muon neutrino). On the other hand, when using the full Hamiltonian, ten additional momentum modes are activated via nonforward scattering processes through the time evolution. We see this effect in Fig. 9 already at early time $t \sim 0.2/\mathcal{E}$. A closer look at the evolution of N_i^- at very early time indicates an acceleration of flavor evolution via nonforward scatterings. We will quantify this acceleration in more detail in the next section by looking at the one-body entropy.

After N_i^- decrease to nearly zero for both full and truncated evolutions around $t \sim 0.5/\mathcal{E}$, N_i^-s show narrower fluctuations with the full Hamiltonian than with the truncated Hamiltonian. In the full evolution, N_i^- (normalized to 1) converges to the equilibrium values (right panel of Fig. 6) quickly and fluctuate around the equilibrium by $\lesssim 0.02$. This is shown in the upper panel in Fig. 10—the black lines are the difference of N_i^- from the microcanonical value, $N_i^- - N_{i,\mathrm{M.C.}}^-$, for all 20 momentum modes and the red line (σ_{N^-}) shows the standard deviation of the difference across the 20 modes. Clearly N_i^-'s converge to the equilibrium values at around $t = 0.5/\mathcal{E}$ and the fluctuate around equilibrium. This is the first evidence we show regarding the equilibration of flavor degrees of freedom in our models. We will further confirm this finding in the next section.

Kinetic randomization of many-body neutrino systems is what we observe only in the presence of the nonforward self-interactions. On the right panel of Fig. 9, we show NN_i^+ for all momentum modes for a 10-neutrino simulation in the Hilbert space $\mathcal{H}_3$—the same initial state as the one shown on the left panel for N^- is used. Our results indicate that momentum mode occupation numbers start fluctuating around asymptotic values for times $t \sim (2\text{–}5)/\mathcal{E}$, depending on the momentum mode. The convergence of N^+ to equilibrium is shown in the lower panel of in Fig. 10—the black lines are the difference of N_i^+ from the microcanonical value for all 20 momentum modes and the red line (σ_{N^+}) shows the standard deviation of the difference across the 20 modes. The deviation of N_i^+ from equilibrium

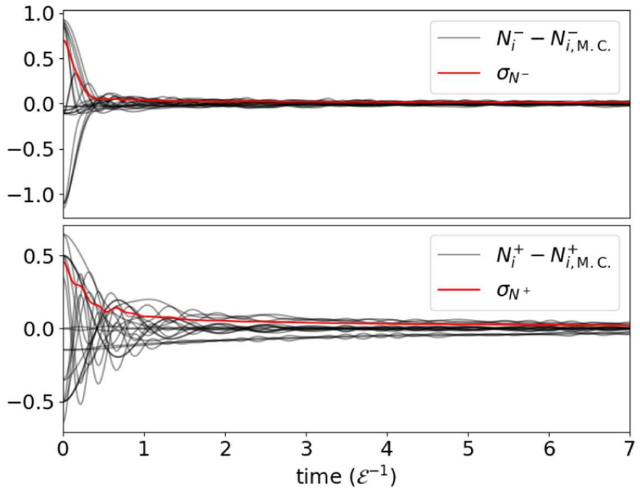

FIG. 10. Top: deviation of N_i^- from the equilibrium values [computed with Eq. (74)] for all momentum modes, along with the standard deviation (σ_{N^-}). Bottom: deviation of N_i^+ from the equilibrium values for all momentum modes, along with the standard deviation (σ_{N^+}). The initial state is the same as the one shown in Fig. 9.

does not appear to drop as quickly as the deviation of N_i^- from equilibrium. This could be attributed to the fact that it takes time for some momentum modes to be populated from a certain initial state due to the smallness of the g factors—an effect that we expect to disappear in larger systems and for initial states with more isotropic momentum distribution.

To summarize, the time evolution of N_i^+ and N_i^- in our model with $N = 10$ neutrinos shown in Fig. 9 demonstrates two things. First, nonforward scattering changes the flavor evolution of the state by activating momentum modes that are initially unoccupied. It appears that the activation of unoccupied modes accelerate the flavor equilibration. Second, even in such a small system of neutrinos, the initial state that is far from equilibrium can kinetically thermalize. The time scales for flavor and kinetic equilibration appear to be both $t \sim O(1)/\mathcal{E}$, and we cannot identify any dependence on the total number of neutrinos N. Further studies will be needed to explore whether a separation of the two time scales arise. Kinetic theory suggests that the time scale for momentum evolution should scale as $t_{\rm inc} \sim (G_F^2 T^5)^{-1}$, in accordance with Fermi's golden rule, while the time scale for coherent refractive effects should scale as $t_{\rm coh} \sim (G_F T^3)^{-1}$. These estimates rely on the assumption (built into kinetic theory) of interactions localized in space and time, which on the many-body side would require working with wave packets, which can be built out of our plane waves basis. If one works with plane waves in a box, as shown in Ref. [13], then the coherent and incoherent time scales become $t_{\rm coh} \sim 1/(\mathcal{E}N)$ and $t_{\rm inc} \sim 1/(\mathcal{E}\sqrt{N})$, respectively. Therefore, we expect that to disentangle the two will require studying larger systems, with $N \sim O(100)$.

E. Entanglement entropy

Finally, we quantitatively assess the time scales of the flavor evolution and kinetic thermalization via the one-body entropies $S(\rho^{(1)})$, $S(\bar{\rho}^{(i)})$ and $S(\rho^{(1,K)})$, which are introduced in Eqs. (49) and (51), respectively. The one-body entropy $S(\rho^{(1)})$ quantifies the entanglement of one neutrino with the rest of the system, and it can be divided to two parts: the kinetic entanglement $S(\rho^{(1,K)})$ and flavor entanglement $(S^{(1),AF} = S(\rho^{(1)}) - S(\rho^{(1,K)})$. In Fig. 11, we show these one-body entropies of a 10-neutrino state over time. The initial state is the same $N = 10$ basis state as the one used in Fig. 9. The black lines show the entropies from the full simulation, while the red lines show those from the truncated evolution. For each Hamiltonian, $S(\rho^{(1)}), S(\rho^{(1,K)})$, and $S^{(1),AF}$ are shown in solid line, dashed line, and dash-dotted line, respectively. At initialization, the flavor component of the entropy, $S^{(1),AF}$, is zero since each neutrino has definite flavor e or μ. On the other hand, since ten momentum modes are occupied, the kinetic component, $S(\rho^{(1,K)})$, starts at a nonzero value. Under the time evolution with the full Hamiltonian, both the kinetic and flavor component of the entropy grow and their sum asymptotes to the maximal value are predicted via the microcanonical ensemble (shown in the blue line). Under the truncated evolution, while the flavor component of the entropy grows over time, the kinetic component stays constant due to the lack of nonforward scattering processes. In this example, the flavor component of the entropy grows at a very similar rate with the full or truncated evolution. We will take a closer look at the difference between flavor evolution under the two Hamiltonians later in the section.

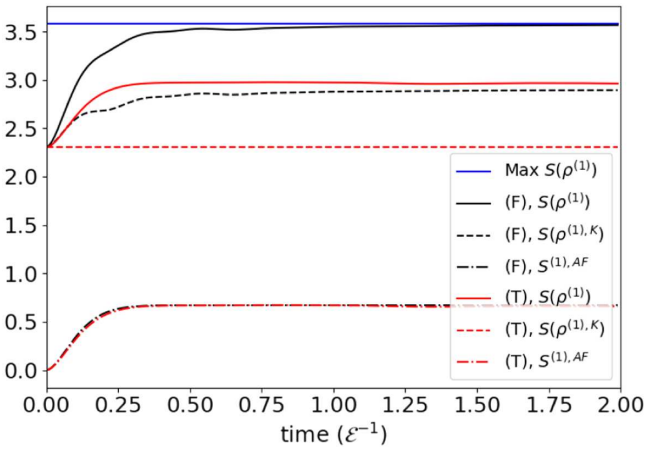

FIG. 11. Time evolution of the one-body entropy $S(\rho^{(1)})$, its kinetic component $S(\rho^{(1),K})$, and flavor component $S^{(1),AF} = S(\rho^{(1)}) - S(\rho^{(1),K})$ for a 10-neutrino basis state. The black lines show the entropies from the time evolution with the full Hamiltonian, while the red lines show the entropies from the time evolution generated by the truncated Hamiltonian. The maximal entropy computed from the microcanonical ensemble is shown by the blue line.

To quantify the time scale associated to the growth of entropy for $N = 6, 8, 10$, we define t_S to be the time when the one-body entropy $S(\rho^{(1)})$ reaches its first maximum. We show t_S and the value of entropy at t_S divided by the maximal value via microcanonical ensemble in Fig. 12 for $N = 6, 8, 10$ neutrinos evolved from the 15 initial states introduced in Sec. VI A. Most notably, for the full simulation shown in circles, most initial states reach over 95% of the maximal entropy around $t_S \sim 0.5/\mathcal{E}$. Interestingly, among the systems we study, we do not see much difference in t_S as the number of neutrino is varied. Note that the initial states will not be able to reach the maximal entropy under the truncated time evolution, as shown by the triangles in Fig. 12. This is because the kinetic component of the entropy cannot be maximized due to the lack of nonforward scattering processes.

To gain insight on the flavor and kinetic equilibration time scales, we look into the kinetic and flavor component of the entropy separately. Regarding the flavor evolution, the flavor component of the one-body entropy is a weighted (by N_i^+/N) sum of the one-mode entropy $S(\bar{\rho}^{(i)})$ as is shown in Eq. (49). Therefore, to remove the information on

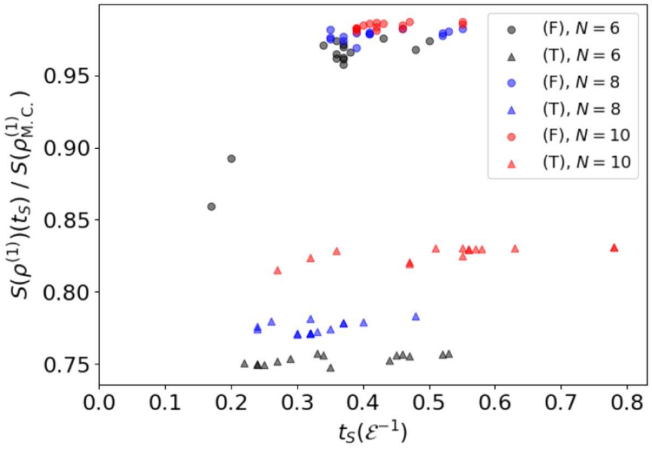

FIG. 12. Time at which the one-body entropy $S(\rho^{(1)})$ reaches its first maximum, t_S, and the entropy at t_S is shown for 15 initial states with $N = 6$ (black), $N = 8$ (blue), or $N = 10$ (red). Circles show the results obtained with the full Hamiltonian, while the triangles show those obtained with the truncated Hamiltonian.

the kinetic randomization, we will first study the one-mode entropy directly. Following that, we will study the time scale of kinetic randomization from the kinetic component $S(\rho^{(1,K)})$ of the one-body entropy.

The entropy of the one-mode (normalized) density matrix $\bar{\rho}^{(i)}$ quantifies the entanglement of neutrinos due to their flavor degrees of freedom. As was hinted via the 2-neutrino toy model in Fig. 2, flavor evolution can be accelerated by nonforward scattering processes since they open up momentum modes that are initially unoccupied, and flavor evolution can take place within those new sectors of the Hilbert space. To illustrate this observation, in Fig. 13, we show the one-mode entropy $S(\bar{\rho}^{(i)})$ over time

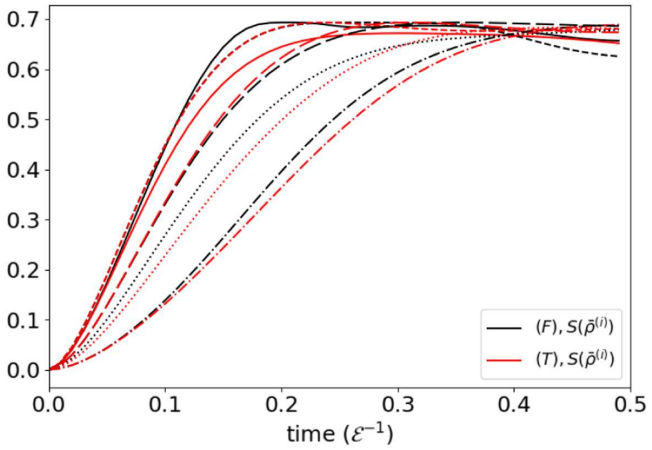

FIG. 13. The entropy per momentum bin, $S(\bar{\rho}^{i})$, is shown for 5 ($\mathbf{z}_1$, $\mathbf{z}_6$, $\mathbf{z}_9$, $\mathbf{z}_{11}$, $\mathbf{z}_{13}$) out of 10 momentum modes that are initially occupied in a 10-neutrino basis state. Black lines show the entropy computed via the full Hamiltonian, while the red lines show those from the truncated Hamiltonian. The line patterns characterize a given momentum bin, regardless of the Hamiltonian used for the time evolution.

for 5 ($\mathbf{z}_1$, $\mathbf{z}_6$, $\mathbf{z}_9$, $\mathbf{z}_{11}$, $\mathbf{z}_{13}$) out of 10 momentum modes that are occupied in the 10-neutrino initial state. The entropy of the wave function evolved under the full and truncated Hamiltonians are shown in black and red lines, respectively. The same line type is used for the entropy of the same momentum mode from the full and truncated time evolution. The figure shows that the entropy grows slightly faster under the full time evolution than via the truncated one (except those in short dashed lines which behave nearly the same for full and truncated evolution).

To quantify the time scale of flavor evolution, we introduce $t_{\bar{S}}$ to be the time when the one-mode entropy reaches 90% of the maximal value, i.e., $0.9 \times \log 2$, for the first time. In Fig. 14, we show the time scales $t_{\bar{S}}^{(F/T)}$ (full or truncated evolution) on the horizontal and vertical axis, respectively, for initial momentum modes in all 15 simulations. Since we focus on the momentum modes in Eq. (73) that are occupied at $t = 0$ and do not count in those that are populated later by the nonforward scattering processes, the total number of data points should be 90 for $N = 6$, 120 for $N = 80$, and 150 for $N = 10$ for both full and truncated setups. However, we discarded those $t_{\bar{S}} > 0.6/\mathcal{E}$, thus 17 ($N = 6$), 20 ($N = 8$), or 9 ($N = 10$) data points from the truncated simulations are excluded from the plots. The distribution of points around the line of $t_{\bar{S}}^{(F)} = t_{\bar{S}}^{(T)}$ in black demonstrates the speedup of flavor evolution via nonforward scattering processes even in these small systems. To show this result even more explicitly, in Fig. 15 we plot the normalized histogram of the ratio $t_{\bar{S}}^{(T)}/t_{\bar{S}}^{(F)}$ for the range [0, 3.25]. The bin with range [0.95, 1.05) is marked with the black vertical line. By comparing the bins on the left and right side of the vertical line, one can clearly see that the nonforward processes affect the time scale of flavor evolution for individual momentum modes and induce a bias towards faster equilibration.

While we observed acceleration of flavor evolution via the full Hamiltonian in our small models, it is difficult to conclude much about the dependence of the time scales on N and k. We will leave a study of flavor evolution time scale with larger number of neutrinos and/or larger number of momentum modes to future work, where we expect to see further speeding-up in the equilibration in the flavor degrees of freedom.

We close the section by demonstrating kinetic thermalization in our neutrino systems evolved with the full Hamiltonian. The kinetic properties of many-body neutrino systems are captured by the occupation numbers N_i^+, and their expected values in equilibrium can be computed from the microcanonical ensemble in Eq. (74). Equivalently, the kinetic one-body entropy $S^{(1,K)}$ should increase over time and asymptote to the maximal value predicted from the microcanonical ensemble as the system equilibrates. In Fig. 16, we show the ratio of $S^{(1,K)}$ to its maximal value in microcanonical ensemble over time for the 15 initial states

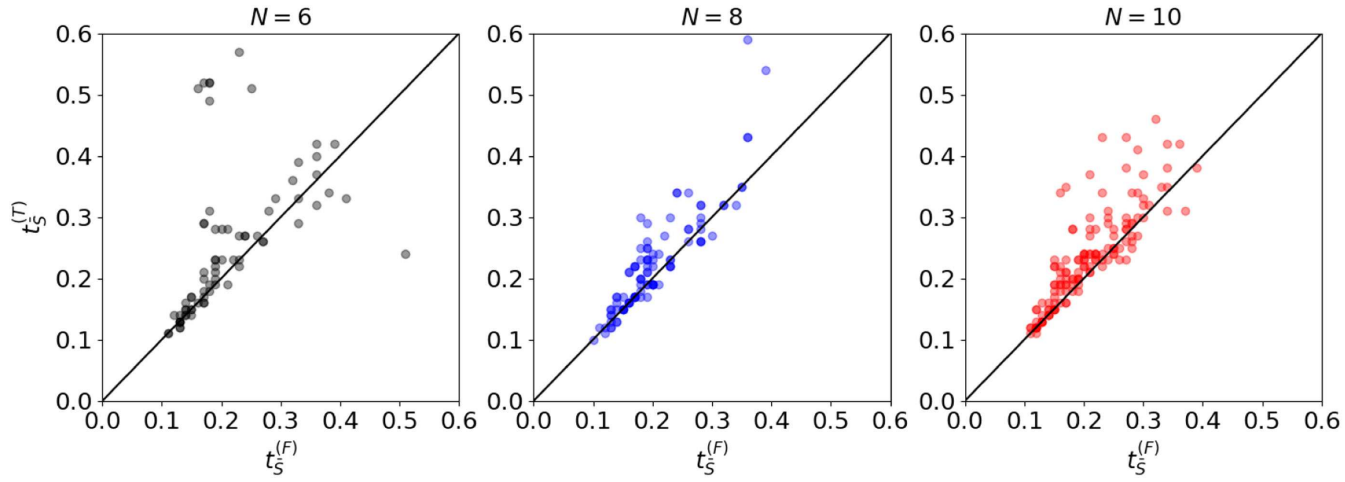

FIG. 14. The time scale $t_{\bar{S}}$ from the full and truncated evolution are on the horizontal and vertical axis, respectively. Results from all 15 simulations and for all momentum modes in Eq. (73) are shown together. The solid lines show the line of $t_{\bar{S}}^{(F)} = t_{\bar{S}}^{(T)}$.

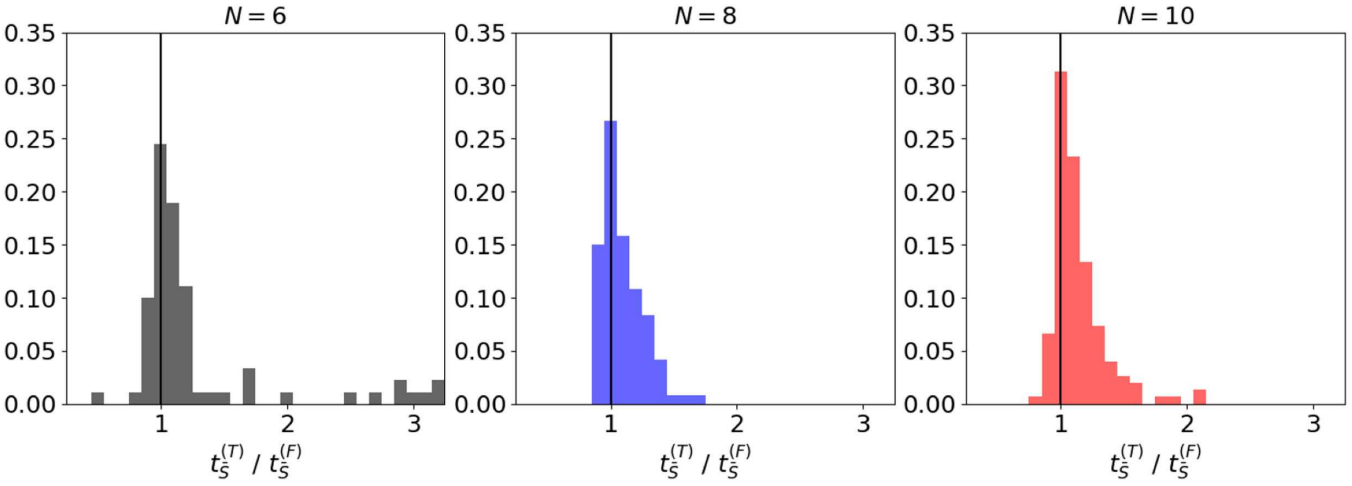

FIG. 15. The histogram of the ratio $t_{\bar{S}}^{(T)}/t_{\bar{S}}^{(F)}$ (truncated/full) in the range < 3.25. Results from all 15 simulations and for all momentum modes in Eq. (73) are counted in together. The histogram is normalized by the total number of counts, that is 90, 120, 150 for $N = 6$, 8, 10, respectively.

in black, blue, and red lines for $N = 6$, 8, 10 cases, respectively. The ratios for $N = 8$, 10 are shifted by 0.1 and 0.2, respectively. The values of $S^{(1,K)}$ in equilibrium are 2.567 for $N = 6$, 2.837 for $N = 8$, and 2.909 for $N = 10$. The systems with six neutrinos have trouble completely thermalizing in our model. On the other hand, we see a nice convergence of the entropy to the maximal value for 8- and 10-neutrino states.

In this section, we analyzed the one-body entropy and the time scales t_S and $t_{\bar{S}}$ that are defined according to the growth of entropy over time. Under the full time evolution, the one-body entropy $S(\rho^{(1)})$ reaches the first maximum for 6, 8, and 10-neutrino systems around $t \sim 0.5/\mathcal{E}$, and we do not see an obvious trend as we vary the number of neutrinos. According to the definition of $S(\rho^{(1)})$, the maximal entropy cannot be achieved using the truncated Hamiltonian due to the lack of nonforward scattering processes. Flavor evolution is where we can directly compare the full and truncated Hamiltonian. First, we show that flavor equilibration demonstrated in Ref. [30] in the forward limit occurs with the full Hamiltonian as well. Furthermore, we show evidence within our models that the full Hamiltonian changes the flavor evolution in the direction of accelerating the equilibration. Thermalization of the momentum distribution is demonstrated in our model, and the time scale for kinetic thermalization appears to be slightly longer than the flavor equilibration time scale. We do not have evidence that these time scales are independent of the models we chose. In particular, the separation of two time scales can vary with the number of

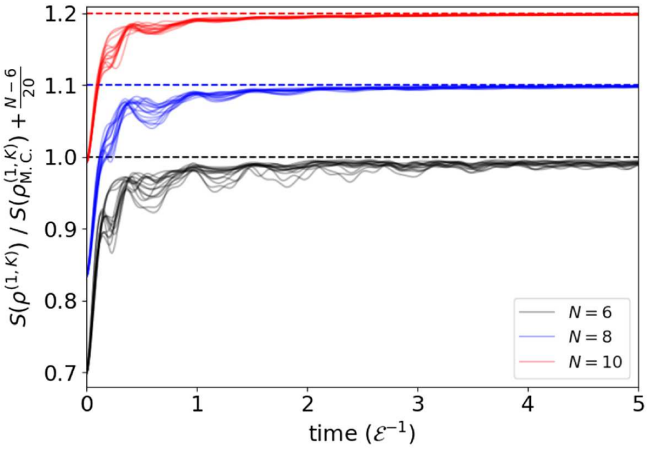

FIG. 16. The ratio of the kinetic component of the one-body entropy, $S^{(1,K)}$, to its maximal value in equilibrium is shown over time for 15 initial states. The lines $N = 8$ (blue) and $N = 10$ (red) are shifted by 0.1 or 0.2 for better visualization. The dotted lines show the maximal entropy predicted from the microcanonical ensemble.

neutrinos or available momentum modes. We leave the study of these time scales with larger number of neutrinos and/or momentum modes to future work.

VII. CONCLUSIONS AND OUTLOOK

In this paper we studied neutrino flavor evolution in the quantum many-body approach using the full neutrino-neutrino Hamiltonian, going beyond the commonly adopted truncated version that allows only for the couplings of neutrino pairs satisfying the forward kinematics condition.

We have set up a framework to implement the time evolution of the system using the occupation number representation for the many-body system. In this setup, we have explored the evolution of simple initial states, i.e. product states of neutrinos with different flavor and momenta. For simplicity, we have restricted the analysis to two flavors. We have studied a toy model with $N = 2$ neutrinos and models with momenta on a two-dimensional grid with $N = 6, 8, 10$ neutrinos and up to $k = 20$ momentum modes. We have quantified the time scales for evolution of flavor and momentum degrees of freedom and their interplay. The main lessons from our explorations can be summarized as follows:

(i) The hierarchy between the neutrino kinetic and potential energy ($T \gg G_F T^3$) results in dynamical pairwise kinetic energy conservation. This is the statement that nonforward terms in $H_{\nu\nu}$, that couple incoming and outgoing pairs of neutrinos, significantly affect the time evolution only when the difference in kinetic energy of the two pairs is on the order of or smaller than potential energy due to the self-interactions. This observation leads to simplifications in the algorithm for time evolution. Moreover, it is worth mentioning that together with three-momentum conservation, for each pair of momenta $\mathbf{p}$ and $\mathbf{q}$ this dynamical kinetic energy conservation still opens up an infinite set of momentum pairs $\mathbf{p}'$ and $\mathbf{q}'$ that contribute to the evolution (see Appendix A). A by-product of this analysis is that one can only see significant differences between full and truncated evolution in systems with spacetime dimension $d > 2$.

(ii) On the qualitative side, we find that nonforward processes affect the dynamics significantly. First, even for the small systems with up to $N = 10$ considered in this study, we find that nonforward processes induce kinetic (momentum) randomization on top of the flavor randomization already induced by the truncated Hamiltonian [30]. We observe "thermalization," i.e. convergence towards expectation values in a suitably defined microcanonical ensemble, in both flavor and momentum on comparable time scales. We also observe that the inclusion of nonforward processes generates a faster flavor evolution compared to the one induced by the truncated (forward) Hamiltonian.

(iii) On the quantitative side, we studied the impact on the evolution time scales using a number of metrics, such as the Loschmidt echo and the entanglement entropy associated with the one-body density matrix. The time scales in all observables are comparable, with $t \sim O(1)/\mathcal{E}$.

In the many-body approach studied in this paper, several open questions remain before one can draw definite conclusions about problems of astrophysical interest, such as assessing the impact of neutrino flavor evolution on nucleosynthesis [42] and on the neutrino signal from galactic supernovae. We can identify several interesting thrusts for future investigations: (i) A key step is the study of systems with larger number of neutrinos (N), which will enable a number of interesting investigations. These include studying the scaling of various observables and time scales with N, exploring the possible emergence of coherent enhancements, e.g. by considering initial states with multiple neutrinos within a given solid angle, and exploring the effect of spatially nonhomogeneous initial conditions (neutrino wave packets). These studies, besides their intrinsic interest, will also help clarifying the connection between the many-body approach and kinetic theory. (ii) Include neutrino-matter interactions in our formalism. This requires the implementation of additional four-fermion operators in the Hamiltonian, which are, however, technically simpler than the one studied here because they are linear or bilinear in the neutrino field. (iii) Implementation on a quantum computer, which requires finding efficient mappings of the full $H_{\nu\nu}$ onto qubit Hamiltonians. (iv) Work towards a comparison with the QKEs, using as common ground the one-body density

matrix. To quantitatively explore the connection of many-body and QKE approaches will require simulating systems with larger number of neutrinos [see point (i) above and discussion at the end of Sec. VI D].

ACKNOWLEDGMENTS

We acknowledge stimulating discussions with Baha Balantekin, Joe Carlson, Huaiyu Duan, Alex Friedland, Julien Froustey, George Fuller, Luke Johns, Scott Lawrence, Gail McLaughlin, Josh Martin, Duff Neill, Amol Patwardhan, Ermal Rrapaj, Sanjay Reddy, Alessandro Roggero, Martin Savage, and Irene Tamborra. We are very grateful to Julien Froustey and Ermal Rrapaj for cross-checking the form of our $H_{\nu\nu}$ with their unpublished work. We also thank Julien Froustey, Luke Johns, Scott Lawrence, Josh Martin, and Duff Neill for providing comments on the manuscript. V. C. and Y. Y. acknowledge support by the U.S. DOE Office of Nuclear Physics under Grant No. DE-FG02-00ER41132. S. S. acknowledges support from the U.S. Department of Energy, Nuclear Physics Quantum Horizons program through the Early Career Award No. DE-SC0021892.

APPENDIX A: KINEMATICS OF $2 \to 2$ SCATTERING

Consider the reaction $\nu_\alpha(\mathbf{p}) + \nu_\beta(\mathbf{q}) \to \nu_{\alpha'}(\mathbf{p}') + \nu_{\beta'}(\mathbf{q}')$. We want to parametrize all the pairs of three-vectors $\mathbf{p}'$, $\mathbf{q}'$ such that $\mathbf{p}+\mathbf{q} = \mathbf{p}'+\mathbf{q}'$ and $|\mathbf{p}|+|\mathbf{q}| = |\mathbf{p}'|+|\mathbf{q}'|$ in terms of $\mathbf{p}$, $\mathbf{q}$, and two angles, denoted below by θ and ϕ. This is achieved by (i) boosting to the center-of-mass system (c.m.s.) of the initial momentum pair $(\mathbf{p},\mathbf{q}) \to (\mathbf{p}_{c.m.s.}, \mathbf{q}_{c.m.s.})$; (ii) parametrizing the outgoing momenta for elastic scattering $(\mathbf{p}_{c.m.s.}, \mathbf{q}_{c.m.s.}) \to (\mathbf{p}'_{c.m.s.}, \mathbf{q}'_{c.m.s.})$ in terms of the polar and azimuthal angles (θ,ϕ) of the unit vector $\hat{v} \equiv \mathbf{p}'_{c.m.s.}/|\mathbf{p}'_{c.m.s.}|$; and (iii) boosting back to the original reference frame $(\mathbf{p}'_{c.m.s.}, \mathbf{q}'_{c.m.s.}) \to (\mathbf{p}', \mathbf{q}')$.

Explicitly, in terms of the c.m.s. velocity $\boldsymbol{\beta} = (\mathbf{p}+\mathbf{q})/(|\mathbf{p}|+|\mathbf{q}|)$, $\gamma = 1/\sqrt{1-\beta^2}$, the unit vector $\hat{v} = (\sin\theta\cos\phi, \sin\theta\sin\phi, \cos\theta)$, and $|\mathbf{p}_{c.m.s.}| = |\mathbf{q}_{c.m.s.}| = \gamma(|\mathbf{p}| - \boldsymbol{\beta}\cdot\mathbf{p})$, one has

$$\mathbf{p}' = |\mathbf{p}_{c.m.s.}|\left(\hat{v} + \boldsymbol{\beta}\left(\gamma + \frac{\gamma-1}{\beta^2}\boldsymbol{\beta}\cdot\hat{v}\right)\right) \tag{A1}$$

$$\mathbf{q}' = |\mathbf{q}_{c.m.s.}|\left(-\hat{v} + \boldsymbol{\beta}\left(\gamma - \frac{\gamma-1}{\beta^2}\boldsymbol{\beta}\cdot\hat{v}\right)\right). \tag{A2}$$

APPENDIX B: HAMILTONIAN INCLUDING ANTINEUTRINOS

In Sec. II we explicitly wrote only the neutrino-neutrino part of $H_{\nu\nu}$, ignoring antineutrinos. Here we will write down all terms in the many-body Hamiltonian, taking into account both neutrinos and antineutrinos. Treating neutrino masses as a perturbation, we only include positive helicity antineutrino modes and use the notation $b_\alpha(\mathbf{p},+) \to b_\alpha(\mathbf{p})$, with $\alpha = e, \mu$.

The kinetic part of the Hamiltonian for the antineutrinos can be obtained by just replacing the $a_{e/\mu}$ by $b_{e/\mu}$ in Eq. (14). When considering the interaction terms, the $\bar{\nu}-\bar{\nu}$ and $\nu-\bar{\nu}$ terms in $H_{\nu\nu}$ are proportional to the same angular function $g(\mathbf{p}',\mathbf{p},\mathbf{q}',\mathbf{q})$ that controls the $\nu-\nu$ interactions. Keeping only the terms that conserve total particle number (i.e. discarding terms that mediate $\nu \leftrightarrow \nu\bar{\nu}\nu$), we find

$$\begin{aligned} H_{\nu\nu} = \frac{G_F}{\sqrt{2}} \sum_{\alpha,\alpha',\beta,\beta'} \int \frac{d\mathbf{q}}{(2\pi)^3}\frac{d\mathbf{q}'}{(2\pi)^3}\frac{d\mathbf{p}}{(2\pi)^3}\frac{d\mathbf{p}'}{(2\pi)^3} g(\mathbf{p}',\mathbf{p},\mathbf{q}',\mathbf{q}) \frac{\delta_{\alpha'\alpha}\delta_{\beta'\beta} + \delta_{\alpha'\beta}\delta_{\beta'\alpha}}{2} \\ \times \Big(a^\dagger_{\alpha'}(\mathbf{p}')a_\alpha(\mathbf{p})a^\dagger_{\beta'}(\mathbf{q}')a_\beta(\mathbf{q})(2\pi)^3\delta(\mathbf{p}+\mathbf{q}-\mathbf{p}'-\mathbf{q}') + 2a^\dagger_{\alpha'}(\mathbf{p}')a_\alpha(\mathbf{p})b_{\beta'}(\mathbf{q}')b^\dagger_\beta(\mathbf{q})(2\pi)^3\delta(\mathbf{p}-\mathbf{q}-\mathbf{p}'+\mathbf{q}') \\ + 2b_{\alpha'}(\mathbf{p}')b^\dagger_\alpha(\mathbf{p})a^\dagger_{\beta'}(\mathbf{q}')a_\beta(\mathbf{q})(2\pi)^3\delta(\mathbf{p}-\mathbf{q}-\mathbf{p}'+\mathbf{q}') + b_{\alpha'}(\mathbf{p}')b^\dagger_\alpha(\mathbf{p})b_{\beta'}(\mathbf{q}')b^\dagger_\beta(\mathbf{q})(2\pi)^3\delta(\mathbf{p}+\mathbf{q}-\mathbf{p}'-\mathbf{q}') \Big). \end{aligned} \tag{B1}$$

[1] B. H. J. McKellar and M. J. Thomson, Oscillating doublet neutrinos in the early universe, Phys. Rev. D **49**, 2710 (1994).
[2] G. Sigl and G. Raffelt, General kinetic description of relativistic mixed neutrinos, Nucl. Phys. **B406**, 423 (1993).
[3] A. Vlasenko, G. M. Fuller, and V. Cirigliano, Neutrino quantum kinetics, Phys. Rev. D **89**, 105004 (2014).
[4] C. Volpe, D. Vaananen, and C. Espinoza, Extended evolution equations for neutrino propagation in astrophysical and

cosmological environments, Phys. Rev. D **87**, 113010 (2013).
[5] J. Froustey, C. Pitrou, and M. C. Volpe, Neutrino decoupling including flavour oscillations and primordial nucleosynthesis, J. Cosmol. Astropart. Phys. 12 (2020) 015.
[6] J. Berges, Nonequilibrium quantum fields: From cold atoms to cosmology, arXiv:1503.02907.
[7] D. N. Blaschke and V. Cirigliano, Neutrino quantum kinetic equations: The collision term, Phys. Rev. D **94**, 033009 (2016).
[8] M. C. Volpe, Neutrinos from dense environments: Flavor mechanisms, theoretical approaches, observations, and new directions, Rev. Mod. Phys. **96**, 025004 (2024).
[9] J. T. Pantaleone, Dirac neutrinos in dense matter, Phys. Rev. D **46**, 510 (1992).
[10] J. T. Pantaleone, Neutrino oscillations at high densities, Phys. Lett. B **287**, 128 (1992).
[11] N. F. Bell, A. A. Rawlinson, and R. F. Sawyer, Speedup through entanglement: Many body effects in neutrino processes, Phys. Lett. B **573**, 86 (2003).
[12] A. Friedland and C. Lunardini, Neutrino flavor conversion in a neutrino background: Single particle versus multiparticle description, Phys. Rev. D **68**, 013007 (2003).
[13] A. Friedland and C. Lunardini, Do many particle neutrino interactions cause a novel coherent effect?, J. High Energy Phys. 10 (2003) 043.
[14] R. F. Sawyer, Speed-up of neutrino transformations in a supernova environment, Phys. Rev. D **72**, 045003 (2005).
[15] A. Friedland, B. H. J. McKellar, and I. Okuniewicz, Construction and analysis of a simplified many-body neutrino model, Phys. Rev. D **73**, 093002 (2006).
[16] B. H. J. McKellar, I. Okuniewicz, and J. Quach, Non-Boltzmann behavior in models of interacting neutrinos, Phys. Rev. D **80**, 013011 (2009).
[17] A. B. Balantekin, M. J. Cervia, A. V. Patwardhan, E. Rrapaj, and P. Siwach, Quantum information and quantum simulation of neutrino physics, Eur. Phys. J. A **59**, 186 (2023).
[18] Y. Pehlivan, A. B. Balantekin, T. Kajino, and T. Yoshida, Invariants of collective neutrino oscillations, Phys. Rev. D **84**, 065008 (2011).
[19] L. Johns, Neutrino many-body correlations, arXiv:2305.04916.
[20] S. Birol, Y. Pehlivan, A. B. Balantekin, and T. Kajino, Neutrino spectral split in the exact many body formalism, Phys. Rev. D **98**, 083002 (2018).
[21] E. Rrapaj, Exact solution of multiangle quantum many-body collective neutrino-flavor oscillations, Phys. Rev. C **101**, 065805 (2020).
[22] M. J. Cervia, A. V. Patwardhan, A. B. Balantekin, t. S. N. Coppersmith, and C. W. Johnson, Entanglement and collective flavor oscillations in a dense neutrino gas, Phys. Rev. D **100**, 083001 (2019).
[23] A. Roggero, Entanglement and many-body effects in collective neutrino oscillations, Phys. Rev. D **104**, 103016 (2021).
[24] A. Roggero, Dynamical phase transitions in models of collective neutrino oscillations, Phys. Rev. D **104**, 123023 (2021).
[25] Z. Xiong, Many-body effects of collective neutrino oscillations, Phys. Rev. D **105**, 103002 (2022).
[26] J. D. Martin, A. Roggero, H. Duan, J. Carlson, and V. Cirigliano, Classical and quantum evolution in a simple coherent neutrino problem, Phys. Rev. D **105**, 083020 (2022).
[27] A. Roggero, E. Rrapaj, and Z. Xiong, Entanglement and correlations in fast collective neutrino flavor oscillations, Phys. Rev. D **106**, 043022 (2022).
[28] D. Lacroix, A. B. Balantekin, M. J. Cervia, A. V. Patwardhan, and P. Siwach, Role of non-Gaussian quantum fluctuations in neutrino entanglement, Phys. Rev. D **106**, 123006 (2022).
[29] J. D. Martin, A. Roggero, H. Duan, and J. Carlson, Many-body neutrino flavor entanglement in a simple dynamic model, arXiv:2301.07049.
[30] J. D. Martin, D. Neill, A. Roggero, H. Duan, and J. Carlson, Equilibration of quantum many-body fast neutrino flavor oscillations, Phys. Rev. D **108**, 123010 (2023).
[31] R. Bhaskar, A. Roggero, and M. J. Savage, Time scales in many-body fast neutrino flavor conversion, arXiv:2312.16212.
[32] B. Hall, A. Roggero, A. Baroni, and J. Carlson, Simulation of collective neutrino oscillations on a quantum computer, Phys. Rev. D **104**, 063009 (2021).
[33] V. Amitrano, A. Roggero, P. Luchi, F. Turro, L. Vespucci, and F. Pederiva, Trapped-ion quantum simulation of collective neutrino oscillations, Phys. Rev. D **107**, 023007 (2023).
[34] M. Illa and M. J. Savage, Multi-neutrino entanglement and correlations in dense neutrino systems, Phys. Rev. Lett. **130**, 221003 (2023).
[35] H. C. Nguyen, B. G. Bach, T. D. Nguyen, D. M. Tran, D. V. Nguyen, and H. Q. Nguyen, Simulating neutrino oscillations on a superconducting qutrit, Phys. Rev. D **108**, 023013 (2023).
[36] P. Siwach, K. Harrison, and A. B. Balantekin, Collective neutrino oscillations on a quantum computer with hybrid quantum-classical algorithm, Phys. Rev. D **108**, 083039 (2023).
[37] S. Shalgar and I. Tamborra, Do we have enough evidence to invalidate the mean-field approximation adopted to model collective neutrino oscillations?, Phys. Rev. D **107**, 123004 (2023).
[38] A. Kost, L. Johns, and H. Duan, Once-in-a-lifetime encounter models for neutrino media: From coherent oscillation to flavor equilibration, Phys. Rev. D **109**, 103037 (2024).
[39] M. A. Nielsen and I. L. Chuang, *Quantum Computation and Quantum Information* (Cambridge University Press, Cambridge, England, 2012).
[40] S. Kullback and R. A. Leibler, On information and sufficiency, Ann. Math. Stat. **22**, 79 (1951).
[41] J. M. Deutsch, Quantum statistical mechanics in a closed system, Phys. Rev. A **43**, 2046 (1991).
[42] A. B. Balantekin, M. J. Cervia, A. V. Patwardhan, R. Surman, and X. Wang, Collective neutrino oscillations and heavy-element nucleosynthesis in supernovae: Exploring potential effects of many-body neutrino correlations, Astrophys. J. **967**, 146 (2024).